Hydride reorientation and its impact on mechanical properties of high burn-up and unirradiated cold-worked stress-relieved Zircaloy-4 and ZirloTM fuel cladding

Quentin Auzoux, Pol Bouffioux, Albert Machiels, Suresh Yagnik, Brice Bourdiliau, Caroline Mallet, Nathanaël Mozzani, Kimberly Colas

Title

Hydride reorientation and its impact on mechanical properties of high burn-up and unirradiated cold-worked stress-relieved Zircaloy-4 and Zirlo™ fuel cladding

Authors

Q. Auzoux[1,4], P. Bouffioux[2], A. Machiels[3], S. Yagnik[3], B. Bourdiliau[1,4], C. Mallet[1], N. Mozzani[2], K. Colas[1,5]

[1] Université Paris-Saclay, CEA, Service d'Etude des Matériaux Irradiés, 91191 Gif-sur-Yvette, France

[2] EDF, R&D, Les Renardières, Ecuelles, F-77818, Moret sur Loing, France

[3] EPRI, 3412 Hillview Avenue, Palo Alto, CA 94304, USA

[4] Now at: Université Paris-Saclay, CEA, Service de la Corrosion et du Comportement des Matériaux dans leur Environnement, 91191, Gif-sur-Yvette, France

[5] Now at: Université Paris-Saclay, CEA, Service d'Etudes Analytiques et de Réactivité des Surfaces, 91191, Gif-sur-Yvette, France

Corresponding author

Quentin AUZOUX

Postal address:

DES-ISAS-DPC-SCCME-LECA

Bâtiment 458, Point Courrier 50

CEA Saclay

91191 Gif-sur-Yvette

Phone: +33 1 69 08 18 34

e-mail: quentin.auzoux@cea.fr

Highlights

- Two cold-worked, stress-relieved claddings were studied: Zircaloy-4 and Zirlo™
- Hydride reorientation (HRO) causes a ductile-to-brittle transition
- No irradiation effect on the HRO critical stress was detected
- Irradiation decreases ductility for a given hydride reorientation state
- Creep-induced cracks in the oxide layer cause preferential hydride precipitation

Abstract

Precipitation of radial hydrides in zirconium-based cladding concomitant with the cooling of spent nuclear fuel can potentially compromise cladding integrity during its subsequent handling and transportation. Complementary experimental programs on unirradiated and irradiated cladding were performed to assess the conditions leading to the precipitation of radial hydrides and their detrimental effects on mechanical properties. This sequel paper to a previous publication [1] presents results for cold-worked, stress-relieved Zircaloy-4 and Zirlo™ cladding used in pressurized water reactors.

Cold-worked, stress-relieved Zircaloy-4 and Zirlo™ behave very similarly, although irradiated Zirlo™ was found to be slightly more prone to hydride reorientation (HRO) than irradiated Zircaloy-4. No distinct irradiation-induced effect on the HRO critical stress was detected. Depending on the initial high temperature that varied from 350 to 450 °C, HRO may cause a ductile-to-brittle transition when the cladding hoop stress, created by internal pressurization of the specimen, ranges from 70 MPa to 120 MPa. Cracking of the oxide layer caused local preferential radial hydride precipitation. The impact of the decreasing temperature and internal pressure during cool-down was also investigated: it has been found that samples undergoing decreasing temperature and pressure cycles are less prone to hydride reorientation.

1 Introduction

During in-reactor operation, the cladding is corroded by the water moderator. Part of the hydrogen created by this redox reaction is absorbed by the zirconium-based cladding alloy. Once the solubility limit of hydrogen in the cladding matrix is reached, hydrogen precipitates in the form of hydride platelets [2]. These hydrides are predominantly aligned in the circumferential and axial directions [3]. Additional circumferential-axial (or simply "circumferential") hydrides precipitate during reactor shutdown due to the decrease of the hydrogen solubility limit with temperature. Fuel assemblies removed from the reactor core are first stored in spent fuel pools. After a few years in wet storage, spent fuel assemblies can be moved into dry storage systems or transported to interim storage facilities prior to reprocessing or final disposal. During the loading operations, including drying of the spent fuel, from the pool to the dry storage or in the transportation cask, the spent fuel heats up due to its decay heat. This results in hydride dissolution, the maximum extent of which will depend on the highest temperature reached by the cladding. Over time, cooling of the cladding occurs following the decrease in decay heat rate and hydride re-precipitation ensues. Hoop stress generated in the cladding by the fuel rod internal pressure can lead to some or all of the re-precipitating hydride platelets in a radial orientation [4]. Precipitation of radial hydrides can lead to additional embrittlement of the cladding [5].

Numerous studies have been performed in the literature on the factors that impact hydride reorientation [6-15]; however, only few of these investigations concern irradiated fuel cladding [16-22]. It was also demonstrated that a threshold or critical stress exists for re-orientation that depends on material condition, the number density of circumferential hydrides already existing prior to precipitation of hydrides and temperature. In the literature, quite different values were reported for this critical stress [7, 11, 13, 15-21].

A previous paper [1] focused on the impact of thermo-mechanical treatments on hydride reorientation and the subsequent possible embrittlement of fuel cladding for irradiated recrystallized Zircaloy-2 cladding with inner liner, commonly used in boiling water reactors (BWRs). The current paper focuses on cold-worked, stress-relieved (CWSR) materials such as those used in pressurized water reactors (PWRs), in particular Zircaloy-4 and Zirlo™. The experimental procedures were similar to those

presented in [1]: unirradiated and defueled irradiated cladding specimens were subjected to various thermo-mechanical treatments with various heating and cooling scenarios under internal pressure. The resulting hydride microstructures were analyzed with an image analysis software and the mechanical behavior was evaluated by ring tensile tests (RTTs). The results are discussed in light of the available knowledge on PWR cladding material.

2 Materials and test conditions

2.1 Materials

2.1.1 Unirradiated materials

The Zircaloy-4 cladding tubes (17 x 17 design) were manufactured by AREVA according to the ASTM specifications. The Zirlo™ cladding tubes were supplied by Westinghouse; tubes originated from two lots manufactured from two different ingots; mechanical tests did not reveal any difference between the two lots. All the chemical compositions of the lots used in this study are given in Table 1. The microstructure of these tubes is typical of a CWSR zirconium alloy.

The specimens, plugged at both ends, were hydrogen-charged by a cathodic process described in [1]. After charging, the samples underwent a thermal treatment under an inert atmosphere at 430 °C for 24 hours and were then cooled at approximately 1°C/min in order to obtain a homogeneous distribution of hydrides across the cladding thickness. Examples of obtained hydride microstructure are illustrated in Figure 1. Hydride platelets are preferentially oriented in the circumferential direction. The hydrogen contents measured by hot vacuum extraction ranged from 260 to 280 wppm for CWSR Zircaloy-4. A wider range was targeted and reached for CWSR Zirlo™ : from 100 to 645 wppm.

Table 1: Chemical composition of the unirradiated materials tested in this study before hydrogen-charging

		Sn (wt%)	Nb (wt%)	Fe (wt%)	Cr	O (wppm)	H (wppm)
Zircaloy-4	**Specification**	1.2 - 1.7	-	0.18 - 0.24	0.07 - 0.13 wt%	-	< 25
	Tubes lot	1.25 - 1.4	-	0.19 - 0.24	0.09 - 0.13 wt%	1080 - 1350	< 8
Zirlo™	**Specification**	0.8 - 1.1	0.8 - 1.2	0.09 - 0.13	< 100 wppm	1050 - 1450	< 20
	Tubes lot 1	0.95 - 1.01	0.84 - 1.08	0.09 - 0.11	55 - 63 wppm	1130 - 1250	8 - 13
	Tubes lot 2	0.92 - 1.04	1.00 - 1.09	0.09 - 0.11	61 - 75 wppm	1150 - 1250	< 8

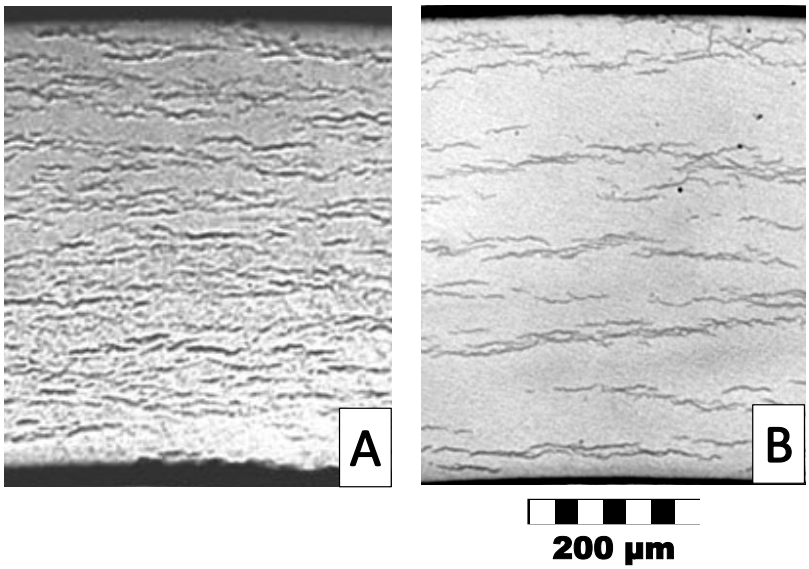

Figure 1: Optical micrographs of cross section of unirradiated cladding after hydrogen-charging; A: CWSR Zircaloy-4 with hydrogen content of ~270 wppm, B: CWSR Zirlo™ with hydrogen content of ~120 wppm

2.1.2 Irradiated materials

CWSR Zircaloy-4 cladding irradiated for five cycles in a French PWR (Cruas 2) was made available for this program through a joint EDF-AREVA-CEA proposal. The reference for the parent fuel rod was FX06FT/B02 and the mean burn-up was 49.2 GWd/MTU. The mean linear heat rate was 9 kW/m during the first cycle and ranged between 16 and 21 kW/m during the remaining four cycles. The nominal outer and inner diameters were 9.50 and 8.36 mm, respectively, giving a wall thickness of 0.57 mm. The Kearns factors for <c> axis crystallographic texture were 0.55, 0.35 and 0.10 for the radial, circumferential and axial directions, respectively. Defueling was performed in warm nitric acid at CEA. Specimens, each about 90 mm in length, were selected at span levels 3, 4 and 6. Hydrogen contents, measured by hot vacuum extraction, were found to range between 160 wppm and 600 wppm at elevation 1200 mm and 2100 mm, respectively. The oxide thicknesses measured on the various samples ranged from 13 µm to 38 µm.

Samples for HRO studies were machined between elevations 1350 mm and 2200 mm. The hydrogen contents determined in the samples studied by image analysis using the Hydruro image analysis software [23] ranged between 250 wppm and 600 wppm, which are values consistent with values of the samples measured by hot vacuum extraction. An example of an initial as-irradiated hydride microstructure at elevation 2100 mm for CWSR Zircaloy-4 is presented in Figure 2 (left). As expected, hydride orientation in the initial, as-received state is mainly circumferential.

Westinghouse supplied CWSR Zirlo™ cladding irradiated in the North Anna PWR for four cycles up to a mean burn-up of 68 GWd/MTU. Cladding outer diameter, thickness and inner diameter were 9.50 mm, 0.57 mm and 8.36 mm, respectively. The Kearns factors for <c> axis crystallographic texture were 0.55, 0.34 and 0.11 for the radial, circumferential and axial directions, respectively. The fuel rods references were AM2-K07 and AM2-H07. The two rods were first part of Assembly AM2 during three cycles of irradiation (mean linear heat rates of 25, 23 and 5 kW/m, respectively) and then part of Assembly 3A4 during a fourth and last cycle of irradiation (mean linear heat rate of 15 kW/m). No particular difference between the two studied Zirlo^{TM}-clad rods was noticed. Defueling was performed at Studsvik and specimens were transported to CEA.

The samples studied in this paper were taken between elevations 1000 mm and 2300 mm. The oxide thicknesses ranged from 18 to 31 µm. The Vickers hardness measured was 292 $Hv_{0.2kg}$ at elevation 1000 mm and 285 $Hv_{0.2kg}$ at elevation 2300 mm. A typical micrograph of the initial as-irradiated hydride microstructure for the CWSR Zirlo^{TM} sample at elevation 2100 mm is presented in Figure 2 (right). Hydrides are mainly located near the outer surface in the form of a hydride rim. The hydride rim is more defined in the Zirlo^{TM} cladding than in the Zircaloy-4 cladding. The overall hydrogen content as measured by image analysis with the Hydruro software for the samples studied ranged from 120 wppm to 420 wppm.

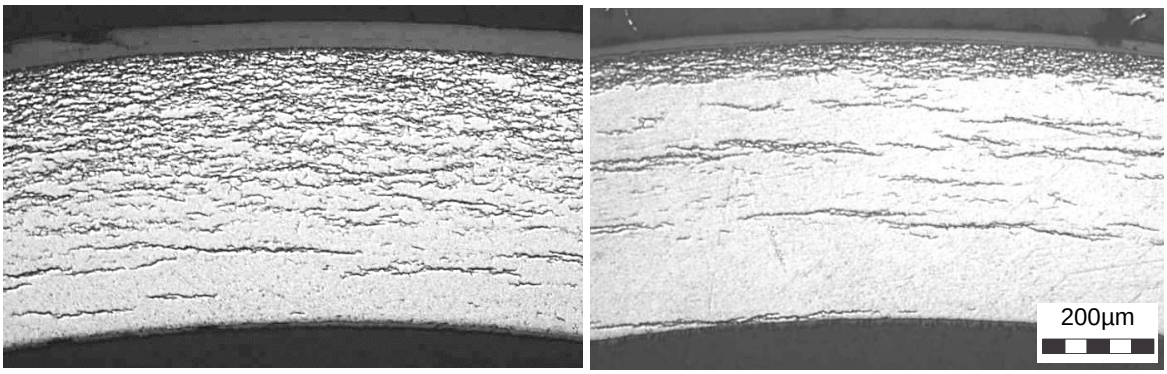

Figure 2: Optical micrographs of cross section of as-received irradiated cladding at elevation 2100 mm, CWSR Zircaloy-4 containing ~600 wppm hydrogen (left), CWSR Zirlo^{TM} containing ~400 wppm hydrogen (right) (Note: the scale is the same for both images).

2.2 Test conditions

2.2.1 Unirradiated, hydrogen-charged materials

The thermo-mechanical treatments performed on unirradiated material consisted of heating the specimens, holding them at temperature for two hours before cooling them under internal pressurization conditions using argon. The specimen lengths ranged from 80 to 120 mm. The tubes were either as-received (i.e., "plain") or machined with four 20-mm long steps of different wall thicknesses. At a given pressure, four different stresses could be obtained with such stepped specimens, thus reducing the number of treatments to study the influence of stress and temperature on hydride reorientation.

After dimensional control (inner and outer diameter), specimens were first heated to the treatment temperature and then pressurized in order to impose the selected effective stress (σ_{eff}) calculated according to Eq. 1, where σ_θ is the hoop stress and σ_r is the radial stress; P is the pressure; OD is the outer diameter of the specimen and ID is the inner diameter.

Eq. 1:

$$\sigma_{eff} = \sigma_\theta - \sigma_r = P\,\frac{ID}{OD - ID} + \frac{P}{2} = P\,\frac{OD + ID}{2\,(OD - ID)}$$

The hoop stress is consequently proportional to the effective stress (Eq. 2).

Eq. 2:

$$\sigma_\theta = \frac{2\,ID}{OD + ID}\,\sigma_{eff}$$

For each sample, the temperature was monitored with three thermocouples ensuring an uncertainty lower than 3 °C. The internal pressure was imposed during the holding and cooling parts of the treatment within ± 0.1 MPa of the set point. The cooling curve obtained according to the furnace inertia followed Eq. 3, where T is the current temperature and T_{max} is the treatment temperature (350 °C, 380 °C, 400 °C, 420 °C or 450 °C).

Eq. 3:

$$T\,(°C) = 25 + [T_{max}(°C) - 25]\,\exp[-\text{time (hours)}/4]$$

Post-treatment characterizations included metallurgical examinations to provide information on the hydride microstructure and mechanical testing to assess material ductility.

The hydride reorientation critical stress is defined as the stress at which hydride reorientation is first observed. This threshold stress value can be estimated from metallographic observations and thus refers only to the observation of the onset of the reoriented hydride microstructure but not to its effect on the mechanical properties.

Mechanical tests were ring tensile tests (RTTs) at room temperature. RTTs were performed on 2-mm large "plain" ring at a crosshead displacement rate of 30 µm/s. The impact of radial hydrides on the mechanical properties was assessed from the Displacement Energy Density (DED) dissipated at failure. For RTTs, the DED corresponds to the area under the engineering stress curve (applied force divided by the initial load-bearing surface) versus the crosshead displacement, expressed in J/mm². To exclude

potential slight difference in overall testing machine stiffness from one test to another, the stress-displacement curves were corrected to impose an elasticity slope of 2 MPa/µm, which is near the actual overall stiffness.

2.2.2 Irradiated materials

The test conditions on irradiated Zircaloy-4 and Zirlo^{TM} were the same as the ones used on specimens of recrystallized Zircaloy-2 with inner liner and are described in detail in [1].

Treatments were done in a machine for creep testing of cladding tube specimens by internal argon pressurization installed in an electric furnace. Irradiated specimens were 35-mm long welded to a piece of unirradiated Zircaloy-4 tubing at one end, which was connected to the pressurization line using Swagelocks and to a Zircaloy-4 end cap at the other end.

Two different thermo-mechanical treatment types were done: Type B and Type C TS. Type B treatments were short-term treatments during which the pressure was maintained constant during cooling. After a 75-minute, constant temperature and pressure plateau, the Type B cooling curve followed Eq. 3, similarly to unirradiated materials. Type B treatments were used to determine threshold stress for hydride reorientation. Compared to Type B treatments, Type C TS treatments were meant to be more representative of actual transportation conditions. "TS" stands for "transportation scenario". Type C TS treatments were longer in duration, and pressure (P) was programmed to decrease linearly with absolute temperature (T in Kelvin) during cooling ($P/P_{max} = T/T_{max}$). The constant temperature and pressure plateaus of Type C TS tested lasted 10 days and the cooling rate was 10 times slower than for Type B treatments. Changes in the outside diameter of the specimens were continuously recorded during the constant temperature and pressure plateau, using a laser extensometer. Creep strain was defined as the variation in external diameter during this plateau divided by the initial external diameter.

The softening due to partial annealing of irradiation defects during thermo-mechanical treatments was estimated from micro-hardness measurements, which were made on metallographic cross sections using a Vickers type indenter under 0.2 kg at mid-thickness locations. 16 measurements were made along the cross-section circumference of each sample. The standard deviation was 5 Hv, which is less than 2 % of the measured hardness values.

Oxide layer thickness, hydride orientation and through-thickness hydride distribution were observed with an optical microscope on metallographic cross sections after etching. Hydrogen content and hydride orientation distribution were then characterized using the Hydruro image analysis software [23]. Up to ~1100 wppm, the uncertainty level for the quantification of hydrogen content with this method is around ± 15 %. Radial hydride fraction is defined as the ratio of radial hydride cumulative length to the total hydride cumulative length. This fraction is expressed as a percentage in the present paper. Multiplying the radial hydride fraction by the hydrogen content (in wppm) gives the radial hydride content (in wppm). More details on the procedure can be found in [1].

To quantify the effect of treatment on cladding mechanical properties, ring tensile tests at room temperature and constant displacement rate (33 µm/s) were performed with an electromechanical tensile frame. The ring samples were spark-erosion machined after removing the inner and outer oxide layers by grinding. Two rings were cut from each treated specimen and tested in the same condition to take into account any variability in the fracture behavior.

3 Results

3.1 Unirradiated, hydrogen-charged materials

3.1.1 Zircaloy-4

The hydride reorientation treatments (HRTs) were carried out at 400 °C on plain tubular specimens under argon internal pressure. The applied effective stresses ($\sigma_{eff} = \sigma_\theta - \sigma_r$) ranged from 40 to 120 MPa. According to the hydrogen content of the samples (260 – 280 wppm) and the terminal solid solubility in dissolution (TSSd) at 400 °C (about 210 wppm [24]), about 75% of the hydrides were estimated to be dissolved at the maximum treatment temperature.

The metallographic examinations (Figure 3) highlight the progressive increase in radial hydrides fraction as the applied treatment stress increases above 70 MPa. These observations appear consistent with the mechanical response of the ring tensile tests at room temperature. Indeed, in Figure 4 presenting the tensile test results for the HRO ring specimens, a decrease in ductility is observed with an increase in treatment stress above 70 MPa. Brittle fracture is observed when the effective stress exceeds 100 MPa.

The displacement energy densities (DED), calculated at ring failure, are plotted versus the treatment effective stress (σ_{eff}) in Figure 5. The behavior is similar to a classical ductile-to-brittle transition. The data could be adequately fitted to a sigmoid function (Eq. 4), where DED_1, DED_2, A_0 and B_0 are constants and σ_{eff} is the treatment effective stress

Eq. 4:

$$DED = DED_1 + \frac{DED_2}{1 + A_0.\exp(B_0.\sigma_{eff})}$$

The best-fit sigmoid function is also plotted in Figure 5. The transition stress, defined as the value of the effective stress where the DED is half of the value of as-hydrided specimens, is around 90 MPa. The material is still considered ductile at the transition stress, recognizing that the definition of brittleness is quite subjective. In this study, the material is considered brittle when the DED curve is reduced to a straight line (no macroscopic plasticity), which corresponds to a DED of roughly 0.15 J/mm² and an effective stress of 100 MPa.

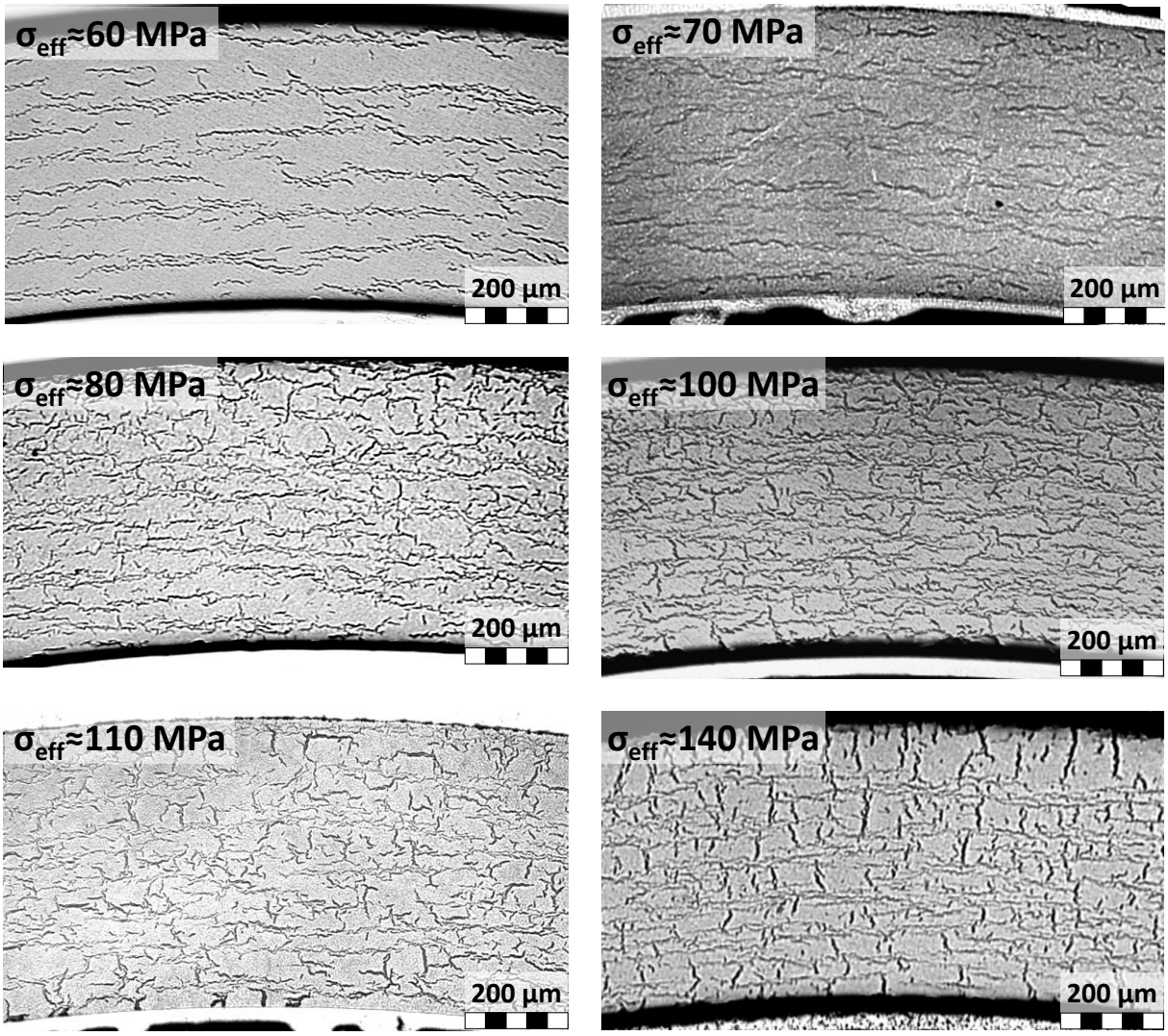

Figure 3: Optical micrographs of cross section of unirradiated CWSR Zircaloy-4 containing ~270 wppm hydrogen after treatment at 400 °C and different effective stresses (Type B treatment).

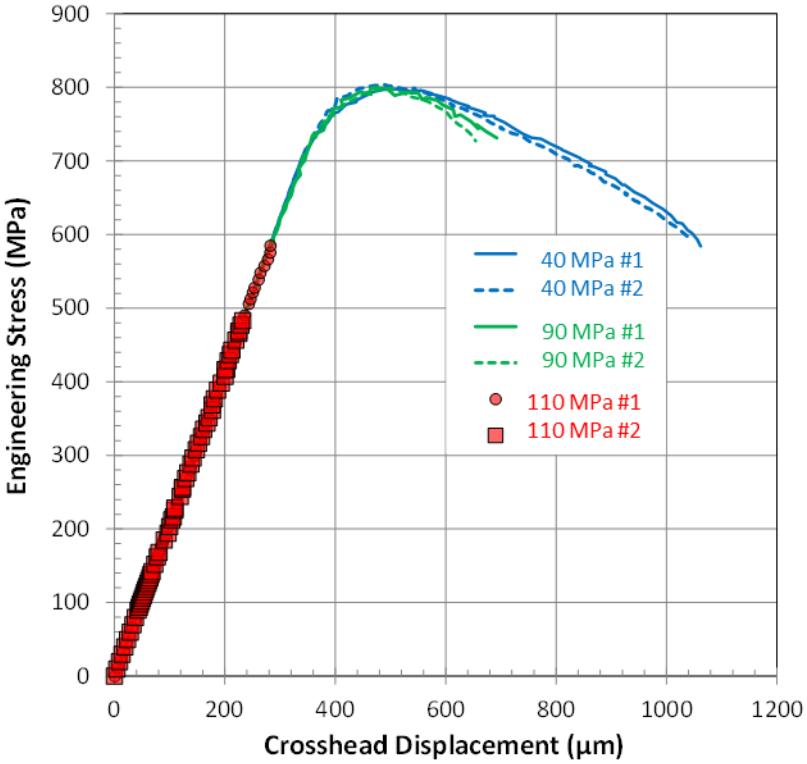

Figure 4: Ring tensile tests at room temperature of unirradiated CWSR Zircaloy-4 containing ~270 wppm hydrogen after Type B reorientation treatment at 400 °C and different effective stresses (40 MPa, 90 MPa and 110 MPa) ; two samples (#1 and #2) were tested for each condition.

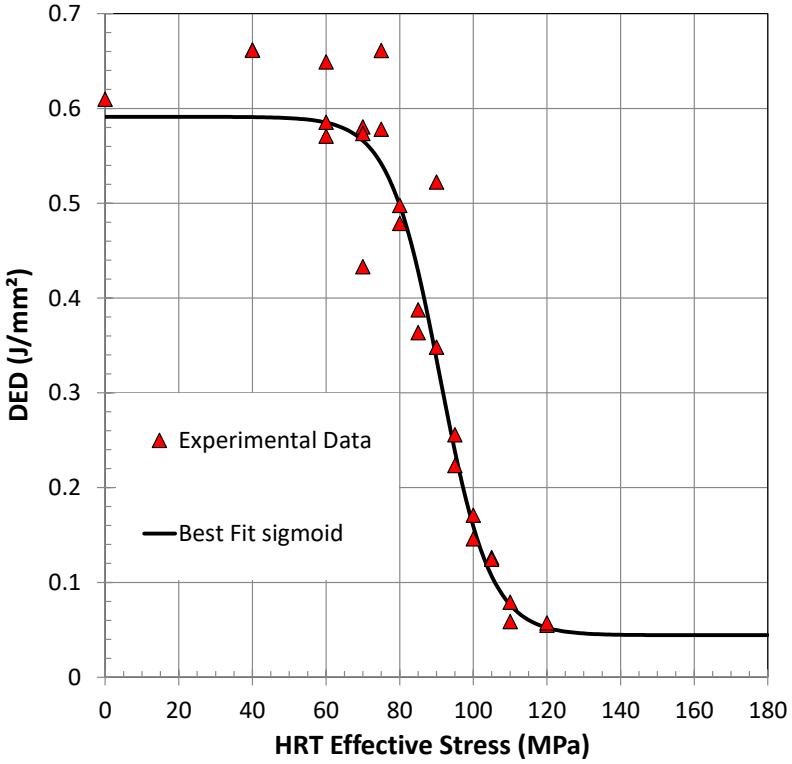

Figure 5: Unirradiated CWSR Zircaloy-4 containing ~270 wppm hydrogen displacement energy density (DED) during ring tensile test at room temperature versus Type B hydride reorientation treatment (HRT) effective stress at 400 °C.

3.1.2 Zirlo™

The thermo-mechanical treatments were carried out under argon internal pressure at four temperatures (350 °C, 380 °C, 400 °C and 420 °C) on the axial step geometry specimen (tube divided in four portions of different external diameters). According to the specific geometry of the specimens, the pressurizing conditions allowed coverage of an extensive range of effective stresses from 60 to 174 MPa. After cooling down and removal of the specimens, rings were cut in each axial zone for metallographic examinations, local hydrogen content measurement and ring tensile tests. The influence of the treatment stress on the hydride reorientation is shown for typical examples in Figure 6 for a treatment temperature of 350 °C (where the TSSd is 132 wppm) and in Figure 7 for a treatment temperature of 420 °C (where the TSSd is 248 wppm). The hydride reorientation critical stress appears to be close to 80-90 MPa, which is slightly higher than for Zircaloy-4.

The DED values calculated at ring failure versus effective stress are presented in Figure 8. Compared to data obtained on Zircaloy-4, more scatter was observed for the Zirlo™ rings but four treatment temperatures were tested. At each treatment temperature, experimental results display a ductile to brittle behavior. For each temperature a best-fit sigmoid was computed. The differences between the fits were minor and it appeared that all the experimental data could be fitted with a single ductile to brittle transition function. The overall best-fit transition sigmoid was computed and exhibited a transition stress close to 105 MPa while it was about 90 MPa for Zircaloy-4. As for Zircaloy-4, a good correlation between an increase of the radial hydride fraction and a decrease of the DED at room temperature was obtained.

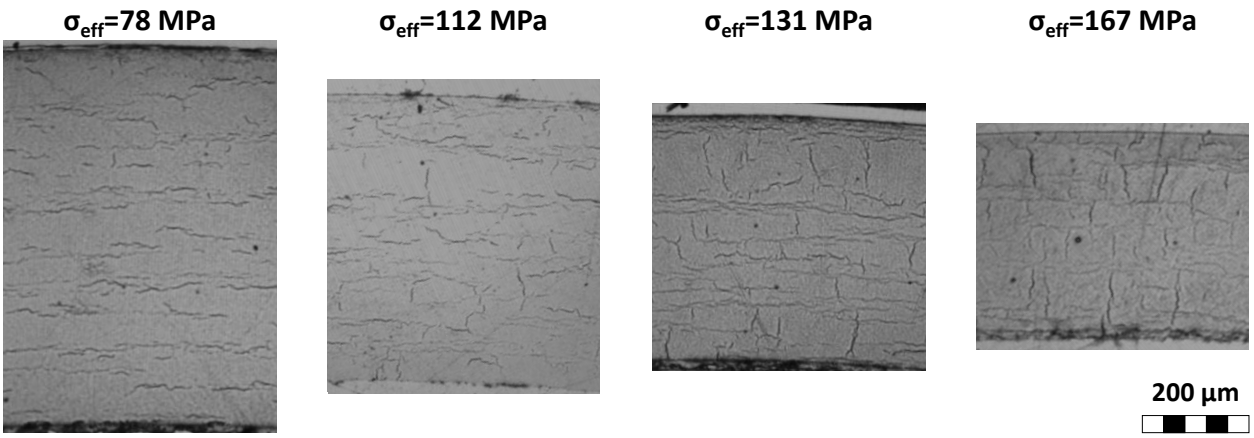

Figure 6: Optical micrographs of cross section of unirradiated CWSR Zirlo™ with intermediate hydrogen content (190-210 wppm) after treatment performed at 350 °C. Higher stresses were attained by using step-thinned specimens.

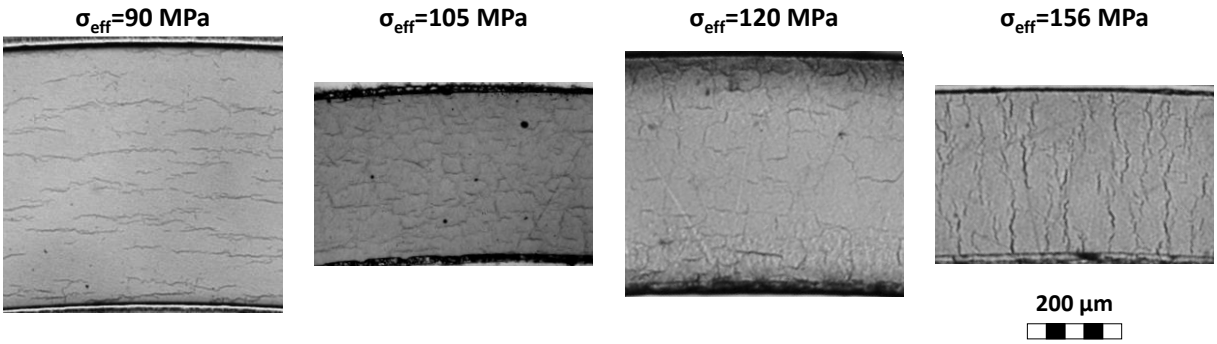

Figure 7: Optical micrographs of cross section of unirradiated CWSR Zirlo™ with intermediate hydrogen content (140-315 wppm) after treatment performed at 420 °C. Higher stresses were attained by using step-thinned specimens.

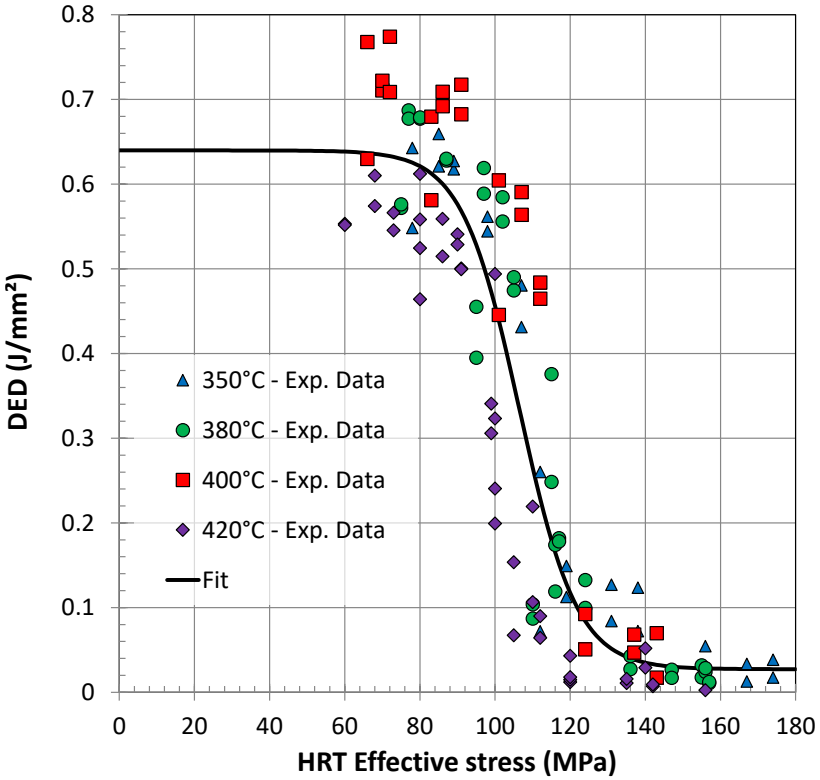

Figure 8: Unirradiated CWSR Zirlo™ DED during ring tensile test at room temperature versus Type B HRT effective stress and temperature. The sigmoid was fitted with the entire set of experimental data.

3.2 Irradiated materials

3.2.1 Zircaloy-4

For Zircaloy-4, two types of treatments at different maximum temperatures and various applied internal stresses were conducted. For the Type C TS treatments, the same theoritical initial pressure at room temperature is applied for both treatments (at 350 °C and at 400 °C), thus the resulting treatment effective stress is 111 MPa for the 350 °C treatment and 120 MPa for the 400 °C treatment. All the test conditions are summarized in Table 2.

Table 2 presents the mid-thickness hardness measurements performed (as mentioned in paragraph 2.2.2) on as-irradiated samples and on irradiated material after the reorientation treatments. As expected, hardness decreases with increase in rod elevation. This is due to the increase in coolant temperature and therefore due to the increase in cladding irradiation temperature with elevation. During Type B treatments, there is a decrease in hardness due to partial irradiation defect annealing. In particular, it can be observed that the higher the treatment temperature, the lower the residual hardness. Treatments at 400 °C and 450 °C led to lower hardness levels: 281 Hv and 259 Hv, respectively, whereas treatments at 350 °C did not seem to affect the initial hardness level (near 295 Hv for this elevation range). The Type C treatments, which are longer in duration than the Type B treatments, led to even lower hardness levels.

Metallographic observations on Zircaloy-4 specimens after Type B treatments at 350 °C, 400 °C and 450 °C are reported in Figure 9, Figure 10 and Figure 11, respectively. Reorientation increases with treatment stress and temperature. From these metallographic observations, the critical effective stress, can be inferred. It lies between 100 MPa and 125 MPa at 350 °C, between 80 MPa and 100 MPa at 400 °C and between 55 MPa and 80 MPa at 450 °C.

Figure 12 shows the metallographic observations made after Type C treatments on Zircaloy-4 specimens. Simultaneous decrease of pressure and temperature during cooling, in contrast to constant pressure during Type B treatments, leads to lower hydride reorientation given the same initial maximum stress and temperature. Only the specimen treated at 400 °C shows significant hydride reorientation. Figure 12 also indicates that the outer oxide layer of this specimen was periodically cracked and that hydrides preferentially precipitated at the crack tips.

The increase in hydride reorientation with increasing effective stress and temperature was quantified by image analysis estimation of both radial hydride content and radial hydride fraction (Figure 13 a and b, respectively). These plots illustrate the progressive nature of the increase in hydride reorientation with stress. It should be noted that the maximum radial hydride content obtained is much lower than the theoretical solubility limit, which is approximately 130 wppm, 210 wppm and 310 wppm at 350 °C, 400 °C and 450 °C, respectively [24].This result indicates that only a part of the dissolved hydrides precipitated into radial hydrides during these treatments. It suggests that additional reorientation would be obtained after higher stress treatments or after multiple thermo-mechanical cycles, as observed by Chu et al. on unirradiated Zircaloy-4 [10].

As shown in Table 2, the hydrogen content of the treated specimens varied from 250 wppm to 600 wppm. Specimens tested at 450 °C, for example, had higher hydrogen content than the ones treated at 350 °C and 400 °C. Consequently, for the same radial hydride fraction, the radial hydride content in the specimens treated at 450 °C is higher than in the others.

Figure 14 illustrates the strong effect of Type B treatment at 350 °C on room temperature mechanical properties: ductility is reduced considerably when the effective stress increases from 80 MPa to 100 MPa; and ultimate tensile strength, which is near 1000 MPa for low treatment stress, decreases to 700 MPa when the effective stress increases to 125 MPa. The DED value consequently decreases from ~0.34 J/mm^2 to ~0.08 J/mm^2 when the effective stress increases from 80 MPa to 125 MPa (Figure 15 a). DED values obtained on specimens treated at 400 °C and 450 °C follow the same trend. DED values for ring tensile specimens tested at room temperature after treatment are plotted versus radial hydride content in Figure 15 b. A clear correlation is obtained. Similar to the unirradiated CWSR Zircaloy-4 situation, hydride reorientation appears to be responsible for the observed ductile-to-brittle transition. Figure 16 illustrates the fact that this ductile-to-brittle transition is associated with a modification of the macroscopic features of the fracture. A significant reduction in the width of gauge length was observed only on specimens with DED values >0.26 J/mm^2. The fracture surfaces of all other specimens appeared – at this observation scale – flat and perpendicular to the applied stress. Some fractures were so brittle that the specimens broke into two parts. One specimen even broke during pre-loading before the tensile test began. On the contrary, when the treatment stress was relatively low, the extent of hydride reorientation was limited (<50 wppm) and the fracture mode was ductile. As shown in Figure 17, the ultimate tensile strength of the corresponding specimens was found to be linearly correlated with hardness; they both decreased when treatment temperature and duration increased because of increasing partial annealing of the irradiation defects that act as obstacles to the motion of dislocations.

Table 2: Hardness and hydrogen content of Zircaloy-4 specimens as-irradiated and after Type B and Type C TS treatments at various temperatures and effective stresses.

Treatment type	**Elevation (mm)**	**Hydrogen content (wppm)**	**Treatment temperature (°C)**	**Effective stress during treatment (MPa)**	**Hardness ($Hv_{0.2kg}$) at mid-thickness**
As-irradiated	1203	180	No treatment	No treatment	307
As-irradiated	2111	630	No treatment	No treatment	292
As-irradiated	2777	550	No treatment	No treatment	287
Type B	1713	280	350	80	290
Type B	1767	350	350	100	296
Type B	1802	330	350	125	300
Type B	1622	390	400	80	278
Type B	1674	390	400	100	282
Type B	1349	360	400	120	284
Type B	2257	560	450	55	254
Type B	1530	580	450	80	261
Type B	1492	540	450	100	263
Type C TS	1858	250	400	120	243
Type C TS	2205	330	350	111	265

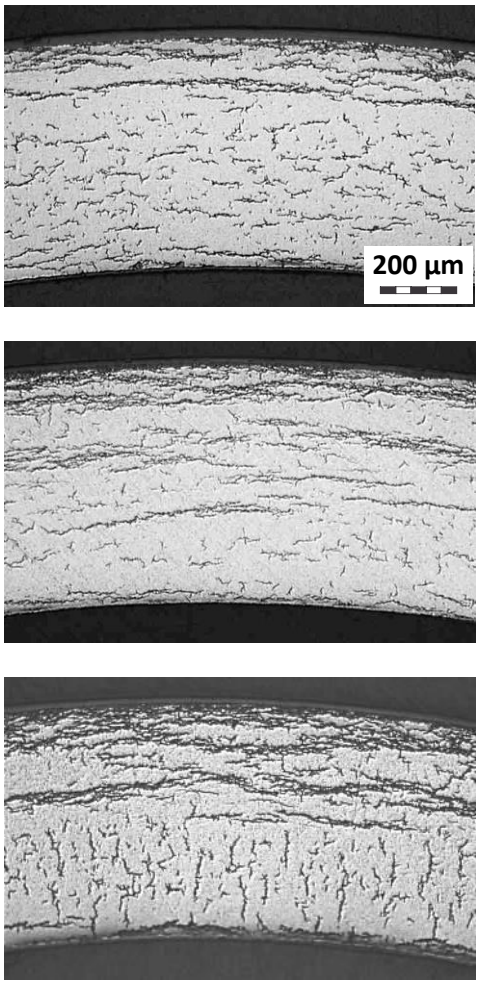

Figure 9: Optical micrographs of cross section of irradiated CWSR Zircaloy-4 containing ~320 wppm hydrogen after Type B treatment at 350 °C and different effective stresses.

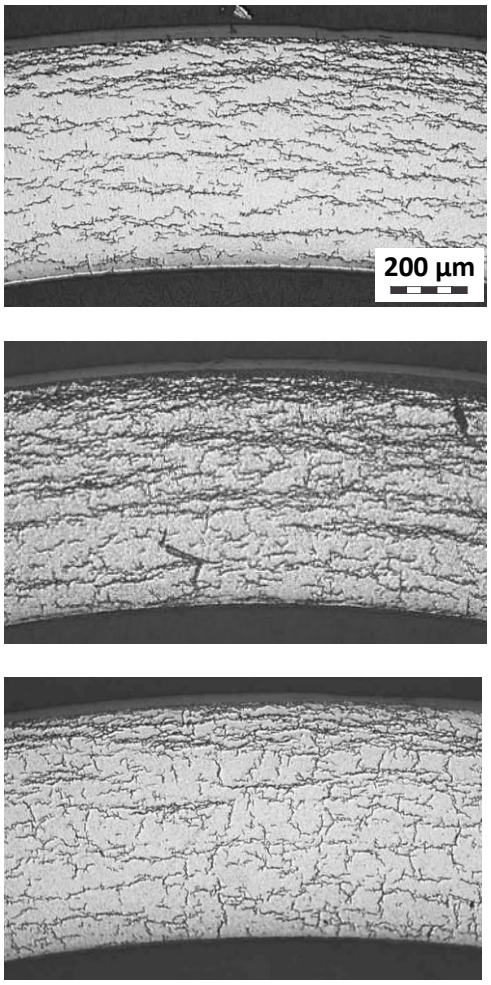

Figure 10: Optical micrographs of cross section of irradiated CWSR Zircaloy-4 containing ~380 wppm after Type B treatment at 400 °C and different effective stresses.

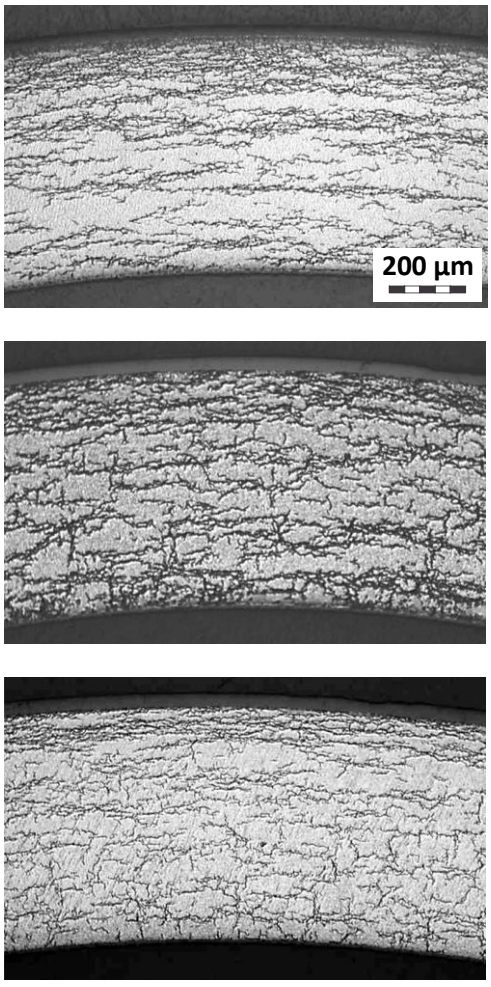

Figure 11: Optical micrographs of cross section of irradiated CWSR Zircaloy-4 containing ~560 wppm hydrogen after type B treatment at 450 °C and different effective stresses.

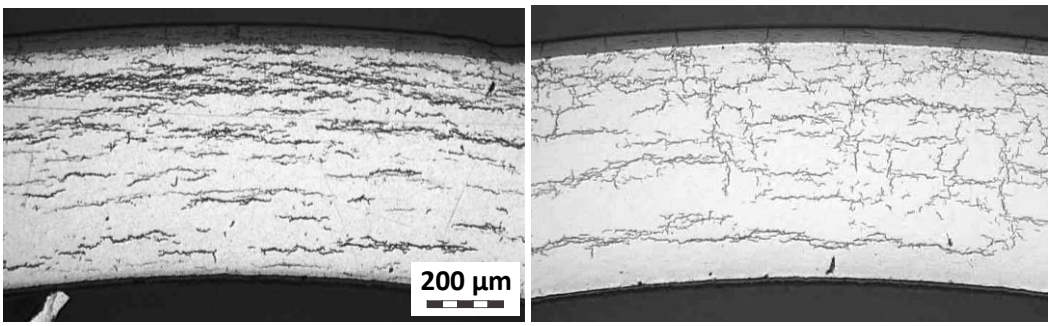

Figure 12: Optical micrographs of cross section of irradiated CWSR Zircaloy-4 containing ~330 wppm hydrogen after Type C TS treatment at 350 °C and maximum effective stress 111 MPa (left), and containing ~250 wppm hydrogen after Type C TS treatment at 400 °C and maximum effective stress 120 MPa (right).

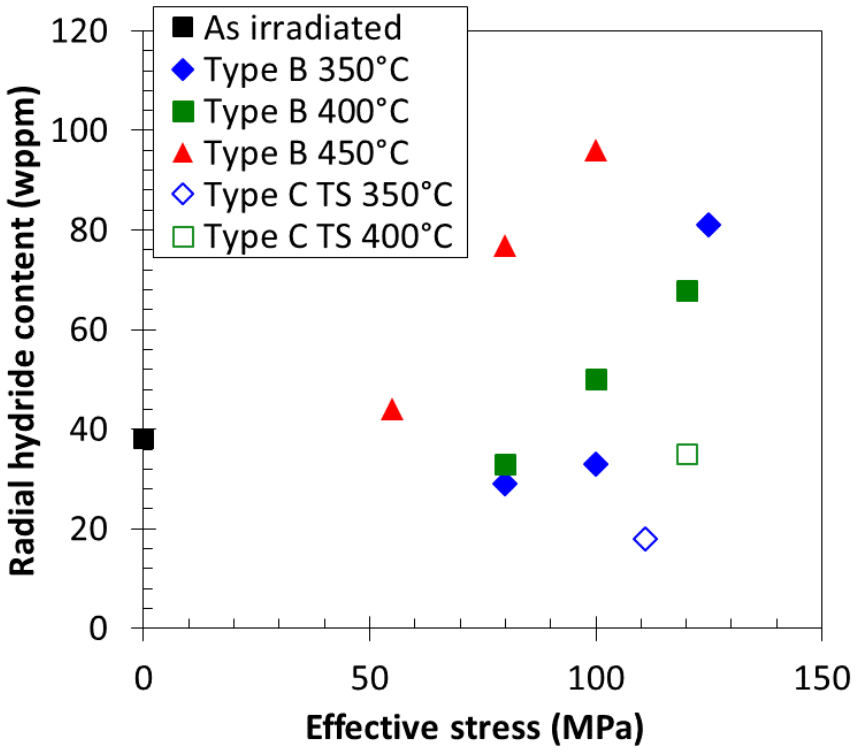

a

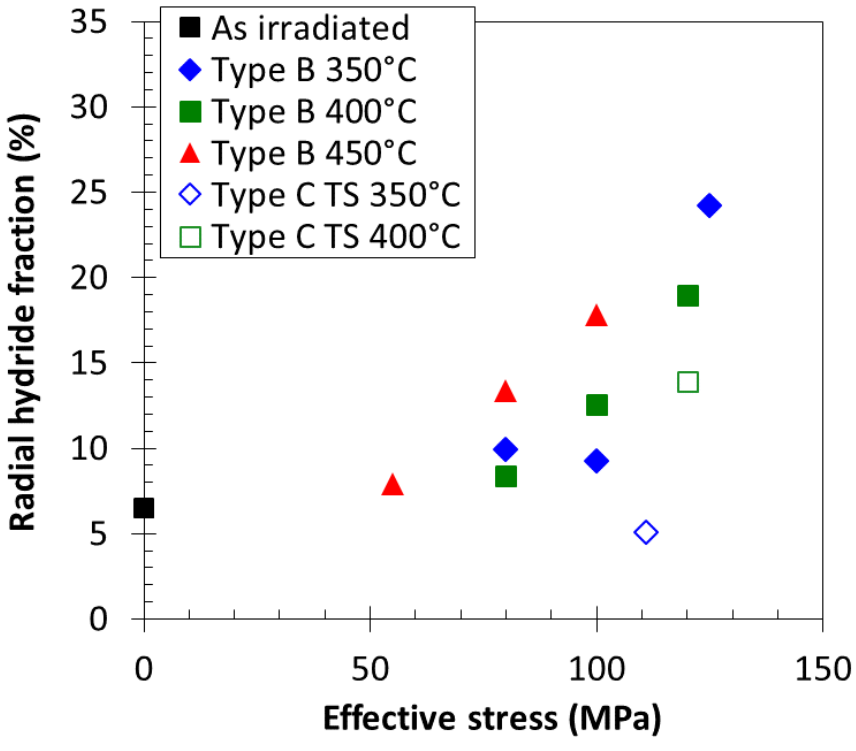

b

Figure 13: Radial hydride content (a) and radial hydride fraction (b) in the initial state and after Type B and Type C TS treatments on irradiated CWSR Zircaloy-4 specimens as a function of effective stress and temperature during treatment.

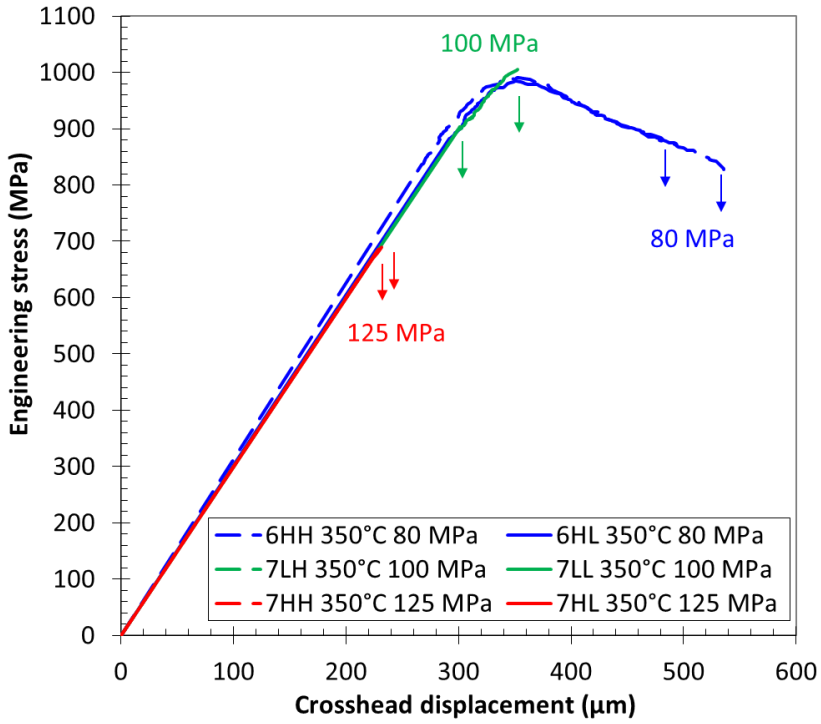

Figure 14: Ring tensile tests at room temperature, irradiated CWSR Zircaloy-4 containing ~320 wppm hydrogen after Type B treatment at 350 °C and different effective stresses (80 MPa, 100 MPa and 125 MPa); Arrows indicate the fracture.

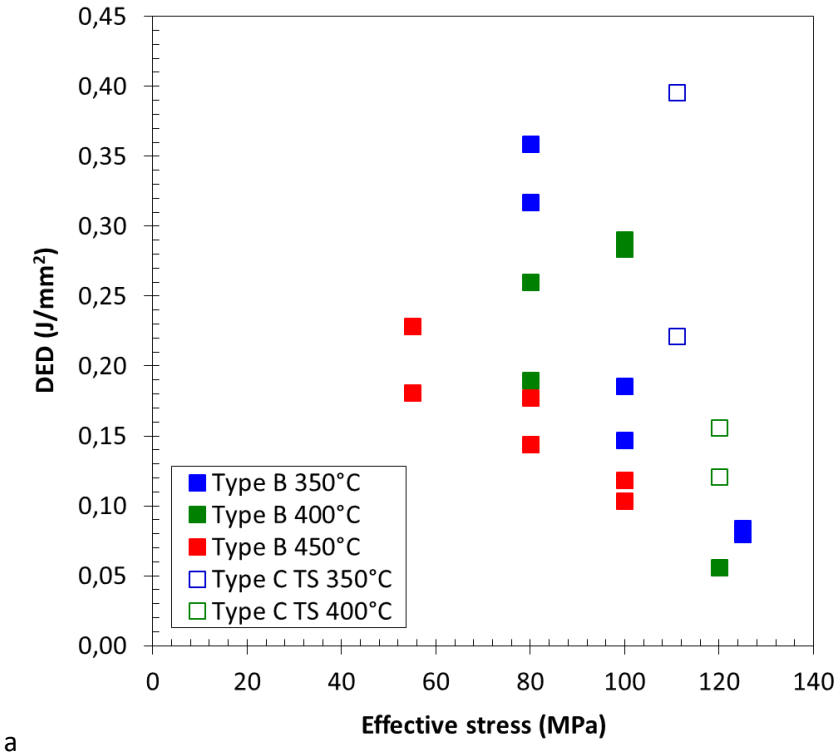

a

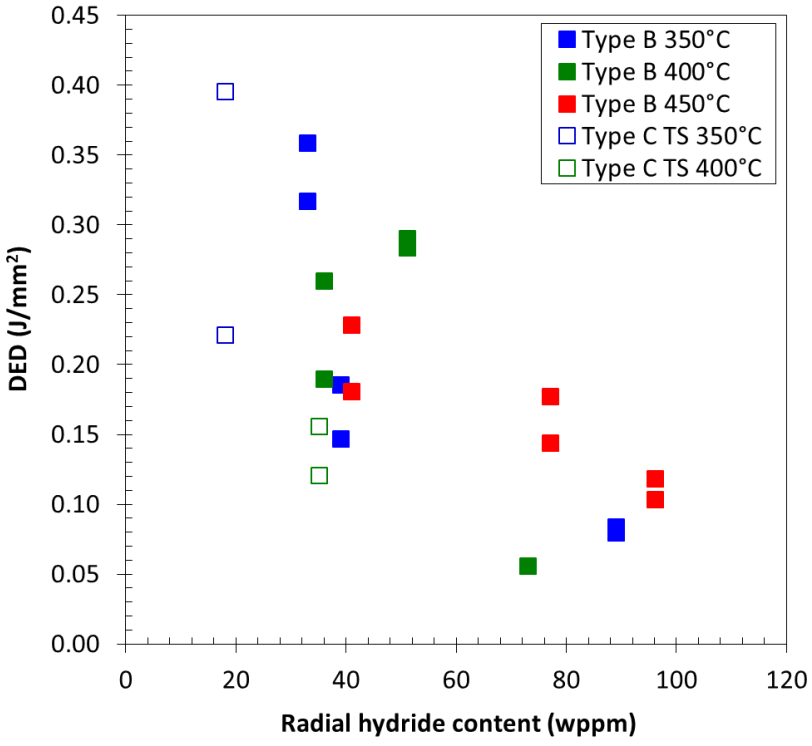

b

Figure 15: Irradiated CWSR Zircaloy-4 DED during ring tensile test at room temperature after Type B and Type C TS treatment versus effective stress (a) and versus radial hydride content (b).

σ_{eff} = 80 MPa 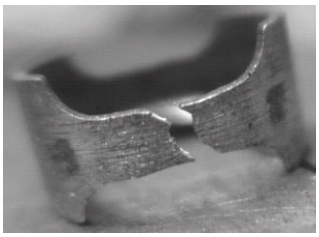

σ_{eff} = 100 MPa 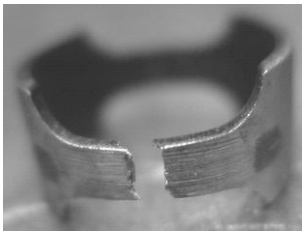

σ_{eff} = 125 MPa 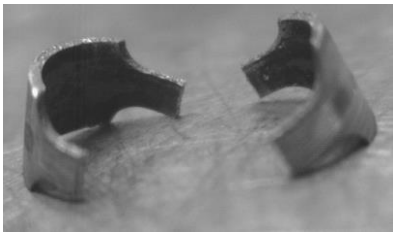

Figure 16: Pictures of fractured specimens after ring tensile testing at room temperature; irradiated Zircaloy-4 containing ~320 wppm hydrogen after Type B treatment at 350 °C and different effective stresses. Nominal dimensions of the ring are given in [1].

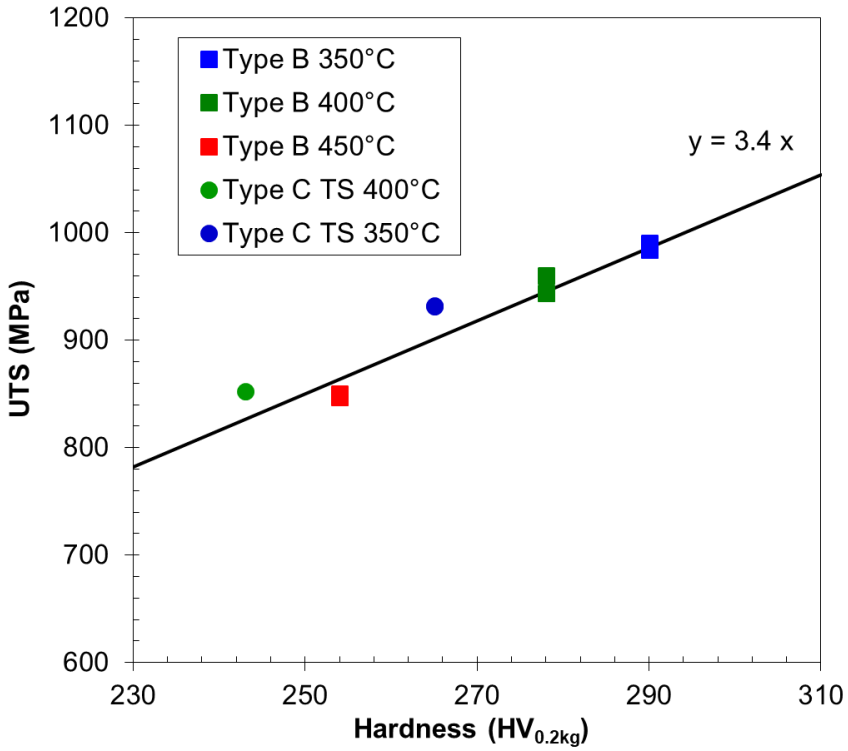

Figure 17: Irradiated CWSR Zircaloy-4 ultimate tensile strength (UTS) during ring tensile test at room temperature after Type B and Type C TS treatment at the lowest studied effective stress versus hardness.

3.2.2 Zirlo™

A summary of the thermo-mechanical treatments conducted on the Zirlo™ samples is presented in Table 3. The chosen treatments are similar to the ones conducted on Zircaloy-4 presented in the previous section. Results from micro-hardness measurements are also presented in Table 3. They are consistent with the results obtained for Zircaloy-4, in particular mid-thickness hardness decreases slightly as rod elevation increases (*i.e.*, as irradiation temperature increases). Due to partial irradiation defects annealing during treatment, hardness was found to be lower in the samples after Type B and Type C treatments than in the initial, as-received state. For Type B treatments, the magnitude of the decrease in hardness was higher after treatment at 400 °C (19 Hv) than after treatment at 350 °C (10 Hv). The relative decreases in hardness due to treatment at 350 °C and 400 °C were 4% and 7%, respectively (which was slightly higher than for Zircaloy-4). The stress level during treatment did not significantly affect hardness. The Type C treatments, which are longer than the Type B treatments, led to even lower hardness levels.

Figure 18 and Figure 19 present the metallographic observations made on Zirlo™ specimens after Type B treatments. Hydride reorientation occurred during the high stress treatments, but not during the low stress treatments. Approximate critical effective stress for hydride reorientation estimated from the metallographs is between 60 MPa and 80 MPa at 350 °C and 400 °C. This critical effective stress is lower than the ones inferred for irradiated Zircaloy-4 specimens. For a given stress, hydride reorientation increases with treatment temperature.

Metallographic observations made on Zirlo™ specimens after Type C treatments are shown in Figure 20. As for Zircaloy-4, a simultaneous decrease of pressure and temperature during cooling (Type C) compared to constant pressure (Type B) leads to less hydride reorientation, given the same initial maximum stress and temperature. Nevertheless, moderate high hydride reorientation was observed after Type C TS treatments at 350 °C and 400 °C. Also noticeable was the enhanced hydrogen redistribution and the almost complete rim dissolution, which only occurred after Type C treatments at 400 °C. The corresponding sample also presented periodic radial cracking of the oxide layers and localized preferential hydride precipitation, whereas the other samples did not.

The increase in hydride reorientation with Type B treatment effective stress and temperature was quantified both by radial hydride content (Figure 21 a) and by radial hydride fraction (Figure 21 b). Hydrogen content of the specimens was in the 225-wppm to 415-wppm range; however, differences were measured from one specimen to another. Specimens treated at 120 MPa and 350 °C, for example, had lower hydrogen content. Consequently, the increase of hydride reorientation with stress was more pronounced in the radial hydride fraction plot (Figure 21 b) than in the radial hydride content plot (Figure 21 a). Similarly to Zircaloy-4, the maximum radial hydride content is much lower than the solubility limit, indicating that additional hydride reorientation is to be expected at higher stresses.

Figure 22 shows the decrease in ductility at room temperature when the stress imposed during the Type B treatment at 350 °C increases. This ductile-to-brittle transition due to hydride reorientation occurs also after treatment at 400 °C. DED plotted versus treatment stress in Figure 23 a illustrates this transition.

DED values from ring tensile specimens tested at room temperature after treatment are plotted versus radial hydride content in Figure 23 b. A correlation is obtained. Increase in radial hydride content is the dominant feature responsible for the observed ductile-to-brittle transition. However, an important scatter is observed. Type-C-treated specimens, for example, have relatively low radial hydride content,

but also low DED values in comparison to Type B specimens. Contrary to Type-C-TS-treated Zircaloy-4 specimens, both Type-C-TS-treated Zirlo™ specimens exhibit brittle fracture. Comparison between Zircaloy-4 and Zirlo™ and comparison of effects from Type B and Type C TS treatments on the mechanical properties at room temperature will be discussed in more detail in the next section.

Figure 24 illustrates the fact that this ductile-to-brittle transition is associated with a modification of the fracture macroscopic features similarly to what was observed with Zircaloy-4 samples. Only specimens treated at 60 MPa show significant reduction in the width of gauge length with DED values above 0.26 J/mm^2. The fracture surfaces of all other specimens appeared – at the macroscopic scale – flat and perpendicular to the applied stress. Some fractures were so brittle that the specimens broke into two parts. One specimen even broke during pre-loading before the tensile test began.

Table 3: Hardness and hydrogen content of Zirlo™ specimens as-irradiated and after Type B and Type C TS treatments at various temperatures and effective stresses

Treatment type	**Elevation (mm)**	**Hydrogen content (wppm)**	**Treatment temperature (°C)**	**Effective stress during treatment (MPa)**	**Hardness ($Hv_{0.2kg}$) at mid-thickness**
As-irradiated	1010	140	No treatment	No treatment	292
As-irradiated	2085	230	No treatment	No treatment	285
As-irradiated	3173	410	No treatment	No treatment	281
Type B	1823	360	350	60	277
Type B	2058	310	350	80	274
Type B	2139	370	350	100	273
Type B	1578	260	350	120	275
Type B	2019	360	400	60	267
Type B	2011	420	400	80	264
Type B	2048	410	400	100	267
Type B	1533	250	400	120	266
Type C TS	2308	240	400	120	242
Type C TS	1785	120	350	111	261

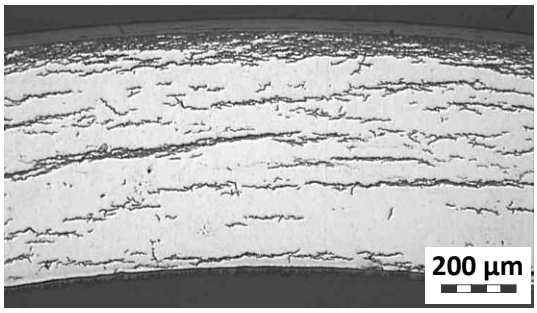

σ_{eff} = 60 MPa

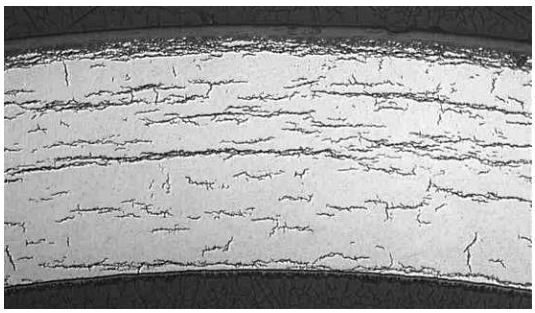

σ_{eff} = 80 MPa

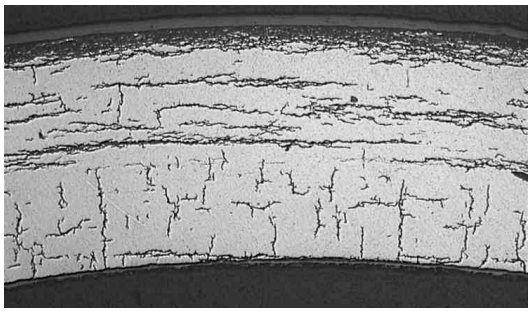

σ_{eff} = 100 MPa

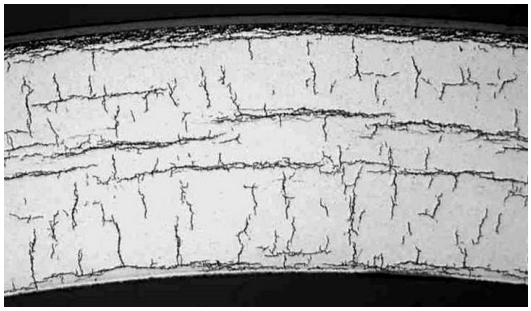

σ_{eff} = 120 MPa

Figure 18: Optical micrographs of cross section of irradiated CWSR Zirlo^{TM} containing ~320 wppm hydrogen after Type B treatment at 350 °C and different effective stresses.

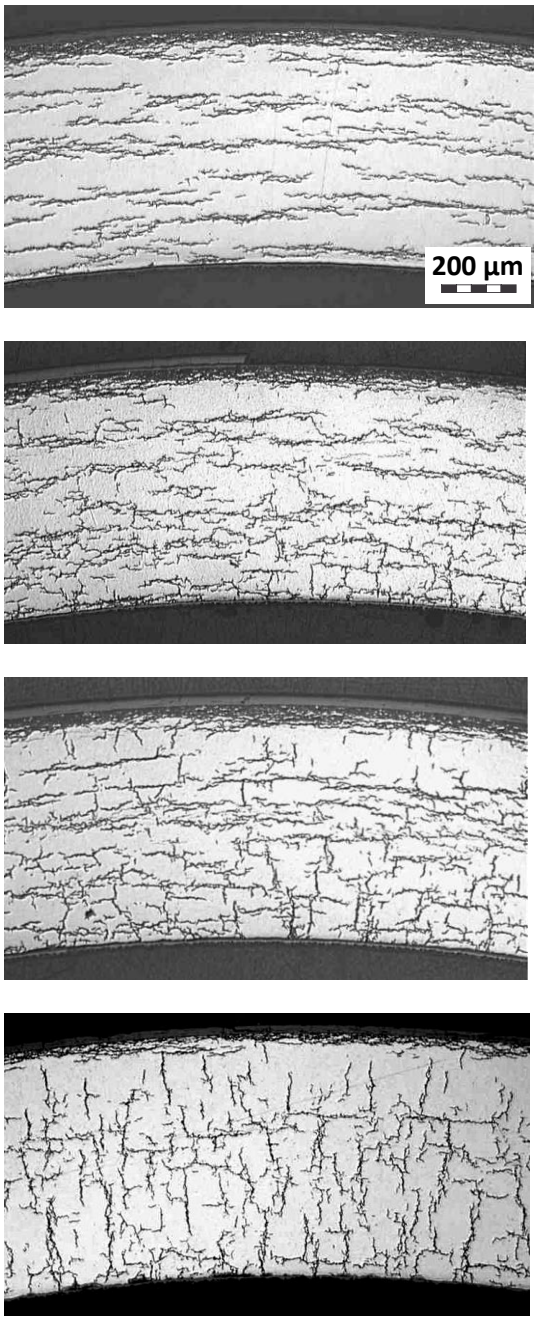

Figure 19: Optical micrographs of cross section of irradiated CWSR Zirlo^{TM} containing ~360 wppm hydrogen after Type B treatment at 400 °C and different effective stresses.

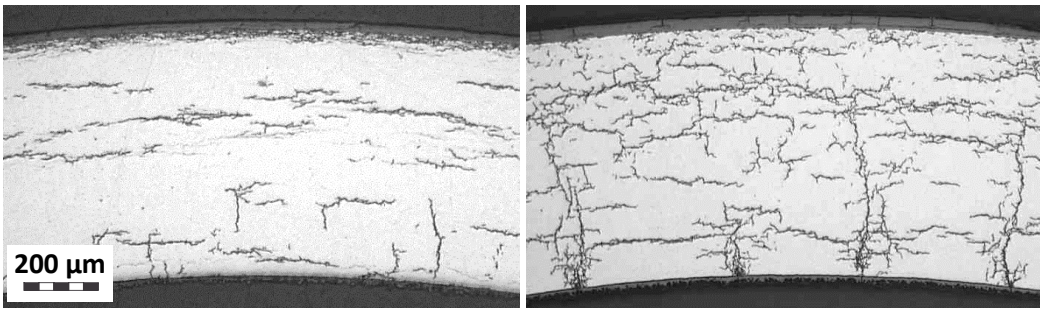

Figure 20: Optical micrographs of irradiated CWSR Zirlo^{TM} containing ~120 wppm hydrogen after Type C treatment at 350 °C and maximum effective stress 111 MPa (left), and containing ~240 wppm hydrogen after Type C treatment at 400 °C and maximum effective stress 120 MPa (right).

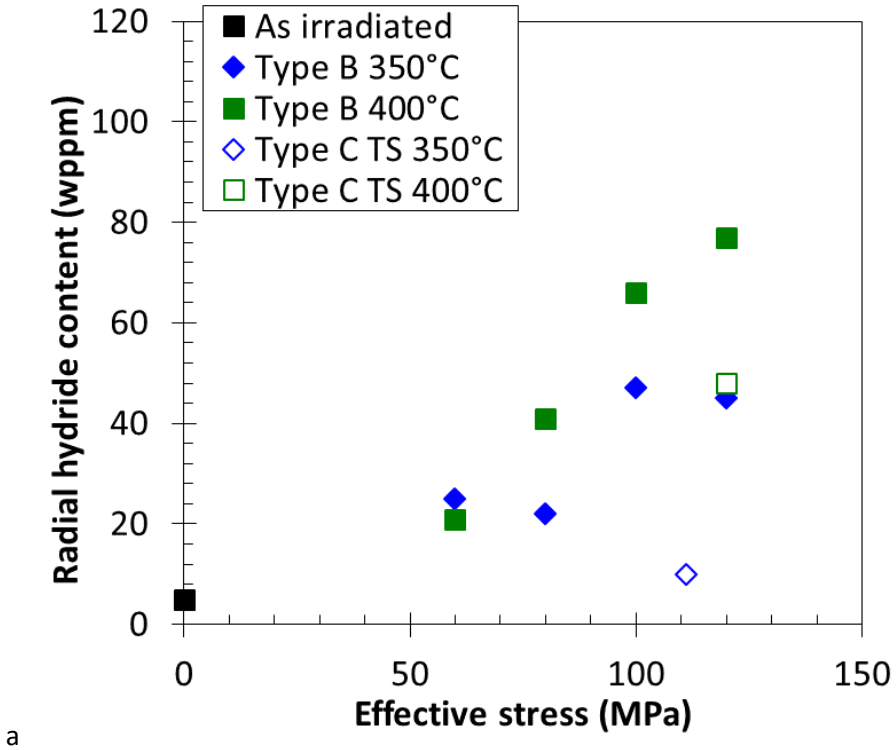

a

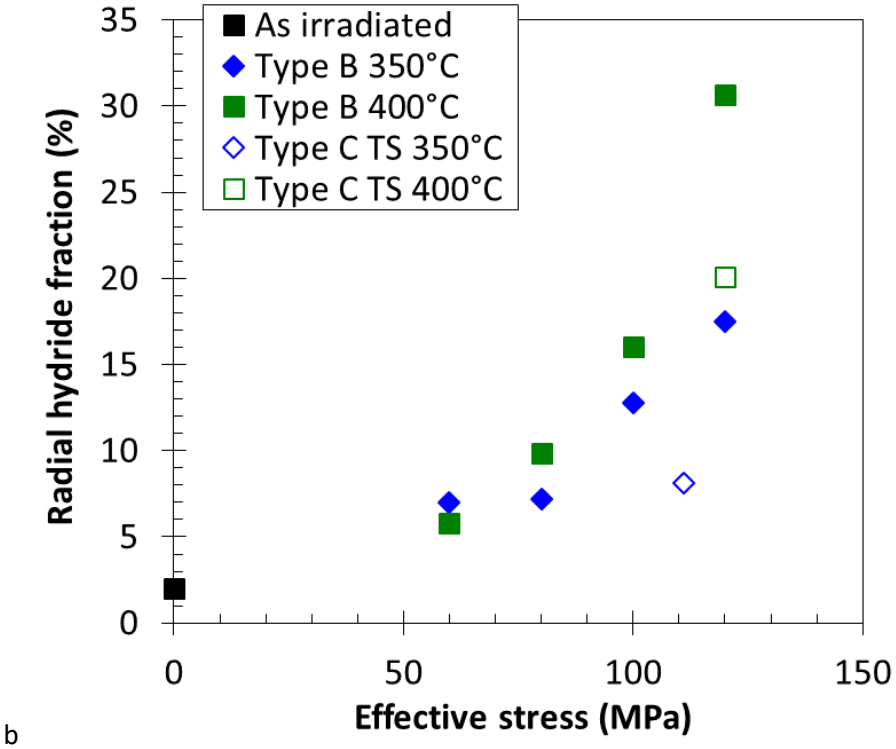

b

Figure 21: Radial hydride content (a) and radial hydride fraction (b) in the initial state and after Type B and Type C TS treatments on irradiated CWSR Zirlo™ specimens as a function of effective stress and temperature.

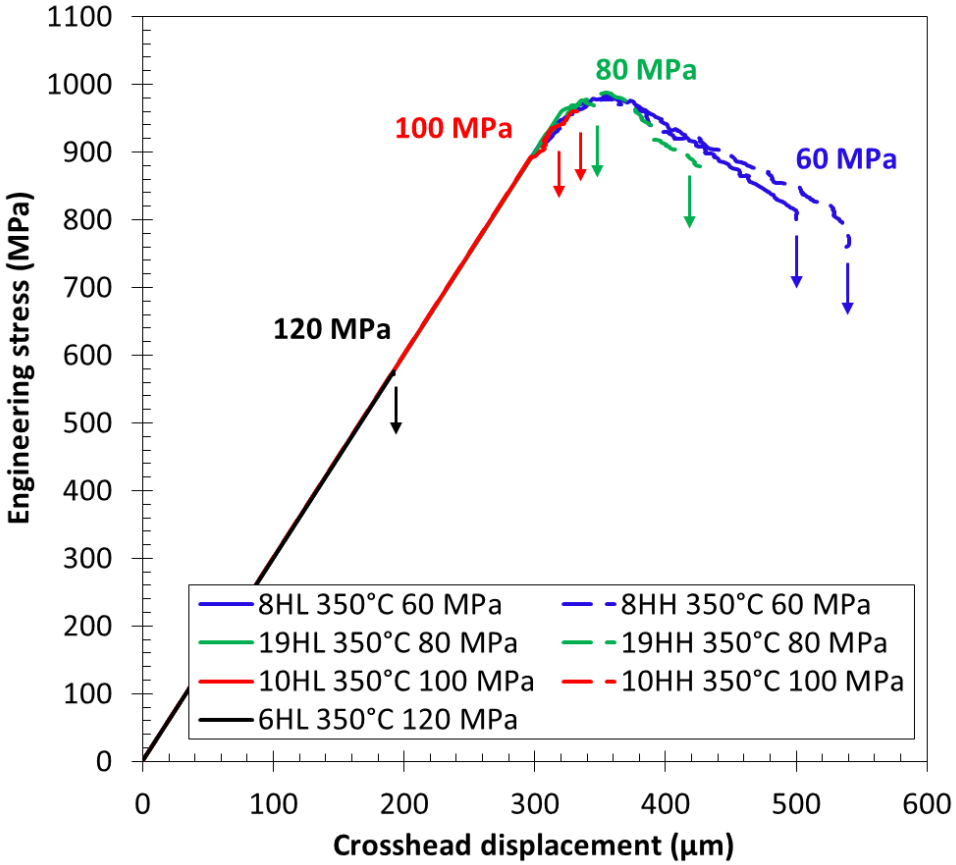

Figure 22: Ring tensile tests at room temperature, irradiated CWSR Zirlo™ containing ~320 wppm hydrogen after Type B treatment at 350 °C and different effective stresses (60 MPa, 80 MPa, 100 MPa and 120 MPa); Arrows indicate the fracture.

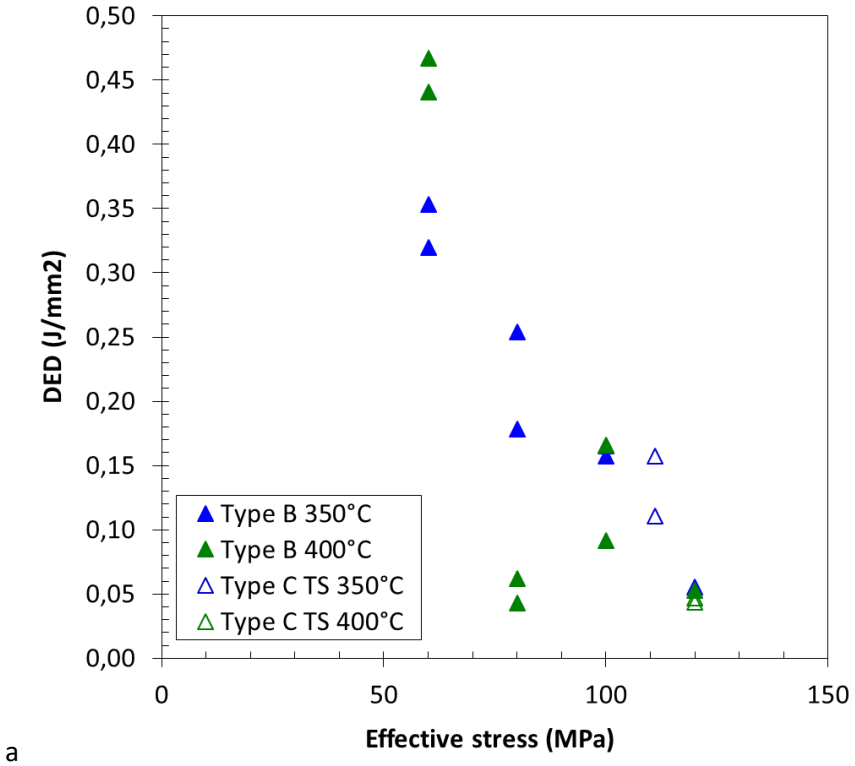

a

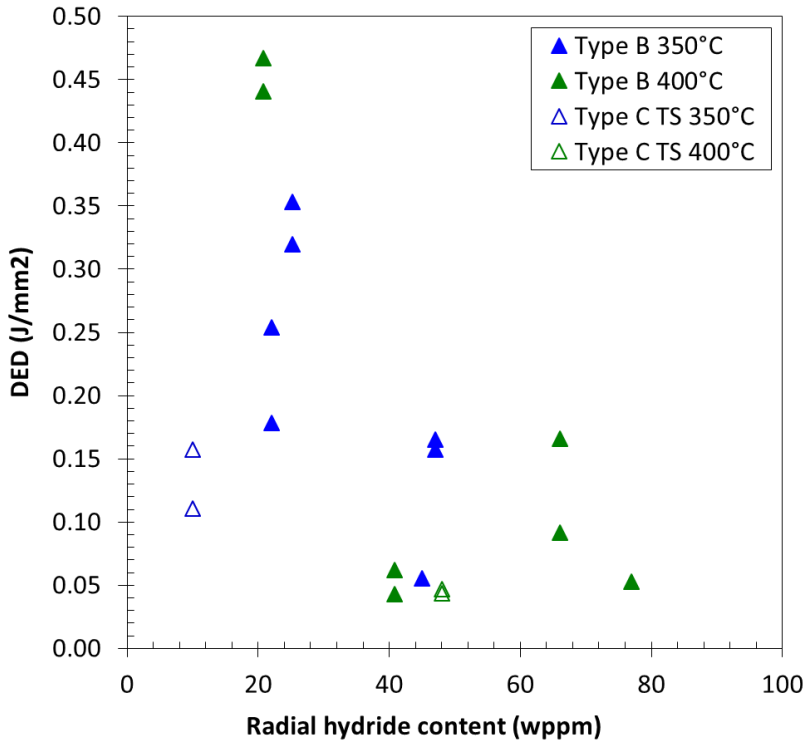

b

Figure 23: Irradiated CWSR Zirlo^{TM} DED during ring tensile test at room temperature after Type B and Type C TS treatment versus effective stress and temperature (a) and versus radial hydride content (b).

σ_{eff} = 60 MPa

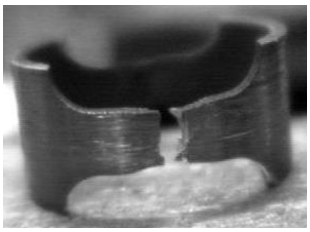

σ_{eff} = 80 MPa

σ_{eff} = 100 MPa

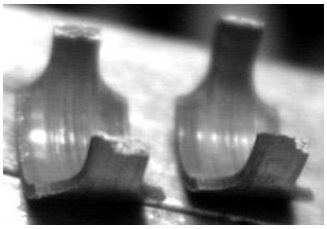

σ_{eff} = 120 MPa

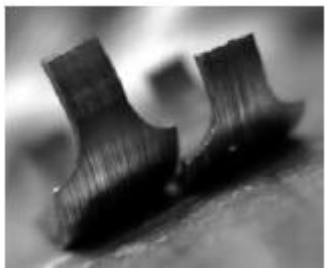

Figure 24: Pictures of fractured specimens after ring tensile testing at room temperature; irradiated Zirlo^{TM} containing ~320 wppm hydrogen after Type B treatment at 350 °C and different effective stresses. Nominal dimensions of the ring are given in [1].

4 Discussion

4.1 Hydride reorientation: irradiation effect and comparison Zircaloy-4/Zirlo™

Although the critical stress for hydride reorientation (HRO) is easily defined, measurements impose subjective qualifications. However, metallographic observations combined with image analysis can provide good estimates of the required minimum stress to detect changes in levels of radially orientated hydrides. To discuss and compare the critical stress for HRO in irradiated and unirradiated claddings, only constant stress (Type B) treatments are considered.

The HRO critical hoop stress of irradiated CWSR Zircaloy-4 lies around 100 MPa at 350 °C, 85 MPa at 400 °C and 65 MPa at 450 °C. This is shown in Figure 25, which includes a data point at 300 °C, obtained from the work of Aomi et al. [19] on irradiated CWSR Zircaloy-4. These results are fully consistent with the conclusion: In the 300-450 °C range, the HRO critical hoop stress of irradiated CWSR Zircaloy-4 decreases approximately by ~15 MPa with each 50 °C increase in treatment temperature. Similarly, an increase in temperature by 50 °C decreases the HRO critical hoop stress by ~10 MPa for irradiated CWSR Zirlo™ between 350 °C and 400 °C. However, for unirradiated CWSR Zirlo™, the HRO critical hoop stress is 85 MPa (± 10 MPa) between 350 °C-420 °C and does not show a similar trend versus temperature.

Figure 25 also underlines the non-detectable irradiation effect on the HRO critical hoop stress of unirradiated CWSR Zirlo™. At both 350 °C and 400 °C, the difference between the critical hoop stress of irradiated and unirradiated specimens is only 5 MPa, which is within the precision of measurements (± 10 MPa). At 400 °C, concerning CWSR Zircaloy-4, the HRO critical stress is slightly higher in the irradiated state than in the unirradiated one (by 15 MPa). As shown in Figure 25, the HRO critical hoop stress of irradiated CWSR Zirlo™ is lower than irradiated CWSR Zircaloy-4 by ~15 MPa. Given that the Kearns factors and the hydrogen content (both in the 250-420 wppm range) of these two claddings are close, the difference in HRO critical stress could be due to a combination of effects of difference in chemical composition, grain size or shape and through-thickness hydride distribution between the two materials.

Due to the relatively narrow range of hydrogen content of the unirradiated CWSR Zircaloy-4 specimens (260-280 wppm), the link between the threshold stress and the hydrogen content cannot be clearly established in our study compared to the one from Lee et al. [15]. Their study of unirradiated CWSR Zircaloy-4 indicates that the HRO critical stress is minimum when the hydrogen content is equal to the TSSd at a given treatment temperature. At 400 °C, it increases from 50 MPa to 80 MPa when hydrogen increases from 200 to 300 wppm. Therefore, the critical hoop stress presently determined for unirradiated CWSR Zircaloy-4 (75 MPa for ~270 wpmm of hydrogen) is fully consistent with their results. Moreover, following the study by Lee et al., we suggest that the 15-MPa difference in the HRO critical stress of unirradiated and irradiated CWSR Zircaloy-4 could be linked to the difference in hydrogen content (~270 wppm in the unirradiated state versus 280-390 wppm in the irradiated one) rather to a potential irradiation effect.

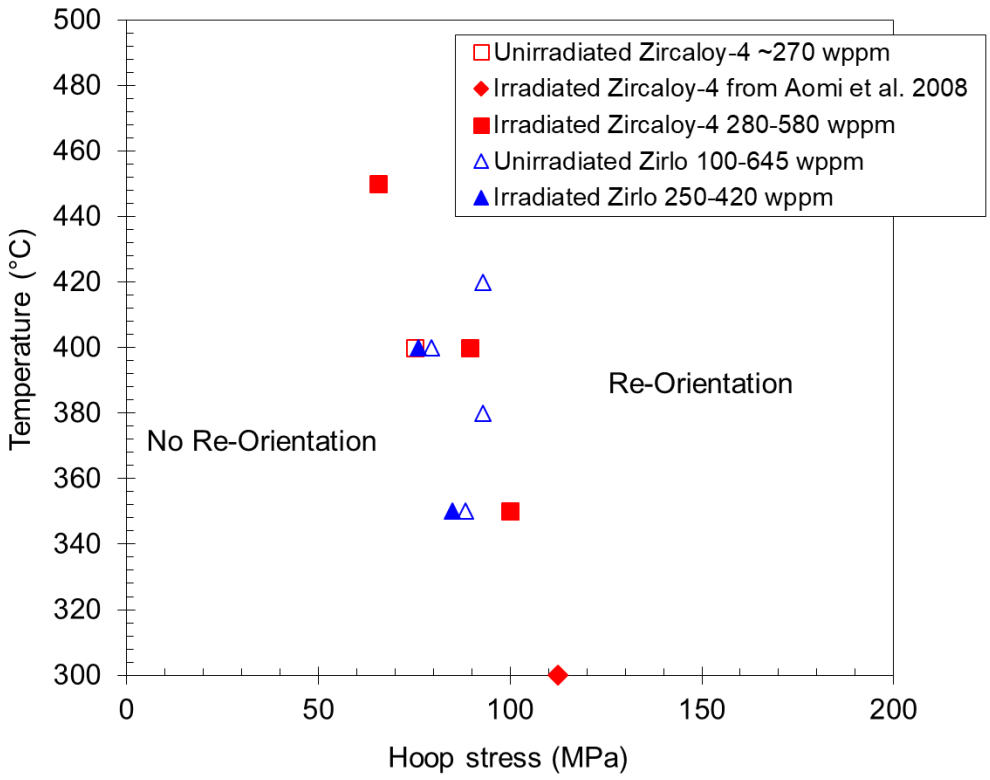

Figure 25: Hydride reorientation critical hoop stress as a function of treatment temperature: (i) obtained after Type B treatment on unirradiated and irradiated specimens (this study); (ii) reproduced from Aomi et al.'s study on irradiated Zircaloy-4 specimens [19].

4.2 Ductile to brittle transition: irradiation effect and comparison Zircaloy-4/Zirlo™

Regarding irradiated and unirradiated CWSR Zircaloy-4 and Zirlo™, the following results are obtained. When the treatment stress is relatively low, the extent of hydride reorientation is limited, and the fracture mode is ductile. When the treatment stress is relatively high, hydride reorientation causes a ductile-to-brittle transition. In spite of the scatter in the results, elongation at fracture, ultimate tensile strength and DED values are clearly found to decrease when treatment stress increases.

Figure 26 compares the DED values obtained on irradiated cladding with those on unirradiated cladding. The ductile-to-brittle transition due to hydride reorientation resulting from Type B treatment at 350 °C and 400 °C occurs in the same range of treatment stress for irradiated and unirradiated CWSR Zircaloy-4 although its HRO critical stress was slightly higher in the irradiated state than in the unirradiated one (Section 4.1). Therefore, irradiation tends to decrease DED for a given hydride reorientation state. A similar trend was observed for CWSR Zirlo™: Although no difference in the critical stress for hydride reorientation was detected in the two conditions for CWSR Zirlo™, a significant shift is seen in the stress range for the ductile-to-brittle transition.

The decrease of DED when the treatment stress increases is slightly steeper for irradiated CWSR Zirlo™ than for irradiated CWSR Zircaloy-4. This fact could be linked to the difference in hydride reorientation behavior between these two materials (Section 4.1). The lower hydride reorientation critical stress for irradiated CWSR Zirlo™ may also be the cause for the low DED values (0.04 and 0.06 J/mm^2) obtained for CWSR Zirlo™ after treatment at 400 °C and 80-MPa and also for the more brittle post-Type C treatment mechanical behavior (Section 3).

These results indicate that not only hydride reorientation level but also through-thickness hydride distribution and irradiation defects may impact ductility. It also underlines the fact that extrapolation from mechanical testing on unirradiated hydride specimens to irradiated specimens may be misleading, particularly since the effect of hydride rims is not taken into account when studying unirradiated samples. Hydride rims are clearly observed in our irradiated CWSR Zirlo™ samples and may impact the hydrogen redistribution and hydride reorientation [25].

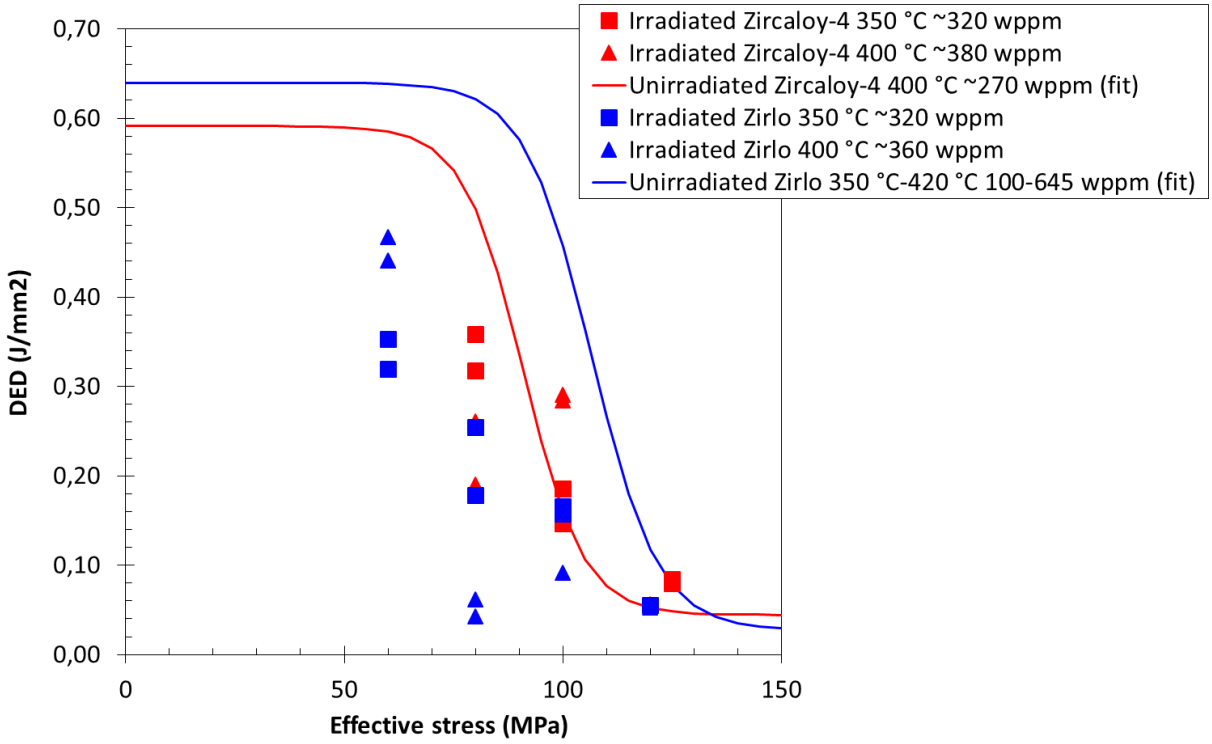

Figure 26: Irradiated and unirradiated CWSR Zircaloy-4 and Zirlo^{TM} DED during ring tensile test at room temperature versus treatment effective stress and temperature. The sigmoids were fitted with the whole experimental data obtained during the present study (see Figure 5 and Figure 8).

4.3 Decreasing pressure and creep strain effect on HRO

The present sub-section aims at highlighting the specifics of Type C TS treatment effects on hydride reorientation in comparison to the simpler, but less realistic, Type B treatments (see the description of the different treatments in section 2.2.2 or in [1]).

As mentioned in section 3.2.1 and 3.2.2, only Type C TS treatments at 400 °C led to periodic cracking of the oxide layers and associated preferential hydride precipitation (Figure 12 and Figure 20). Table 4 sums up the metallographic observations made on Zircaloy-4 and Zirlo™ regarding oxide fracture, preferential hydride precipitation at oxide crack tips and creep strain. The increase in duration and temperature at the plateau is found to correlate well with creep strain, oxide fracture frequency and localized hydride precipitation. Relatively low creep strain (~0.17%) appears sufficient to produce oxide cracking and therefore stress concentration, which causes local radial hydride precipitation. Consequently, the synergistic effects of creep on hydride reorientation may have to be considered when dealing with applications to spent fuel management.

The nucleation of hydrides during cooling occurs at a lower temperature than their dissolution; this phenomenon is called the dissolution precipitation hysteresis [26, 13]. Using synchrotron X-ray diffraction, several authors show that the hysteresis is even more important for the nucleation of radial hydride than for circumferential hydride [27, 28]. Consequently, the stress at onset of hydride precipitation and subsequent cooling in Type C TS treatment, compared to Type B treatment, decreases by ~10% because of the simultaneous and proportional decrease in pressure as a function of absolute temperature. Moreover, depending on the initial stress, stress during cooling may stay below the HRO critical stress long before hydride precipitation is complete. For a given maximum stress and temperature, Type C treatments are consequently expected to lead to lower radial hydride levels than Type B treatments. Results obtained on Zircaloy-4 and Zirlo™ confirmed this expectation (Figure 13 and Figure 21). One should however note that a fraction of the hydrogen dissolved during the C-TS experiments may have more time to migrate and thus to precipitate in the sample end caps. This effect is minimal in our experiment since the hydrogen content as measured after treatment is not significantly lower than the one measured prior to the experiment on sister samples. The dissolution precipitation hysteresis therefore provides a beneficial margin, to reduce or possibly eliminate reorientation, when the stress decreases with temperature during cooling. Recent works [29, 30] have shown that, in the absence of applied stress, the hysteresis effect may be much less important when pre-existing hydrides remain during dissolution, which is the case for the most external part of our samples. In this part, hydride growth rather than hydride nucleation could be favored, especially at low cooling rate. This would imply that potentially fewer hydrides would be available for reorientation for cladding with higher hydrogen contents compared to those with lower total hydrogen contents that would be fully dissolved at high temperature and thus present a stronger hysteresis effect upon cooling.

When comparing the results from the Type C treatment obtained on Zircaloy-4 and Zirlo™ samples to those obtained on Zircaloy-2 samples in [1], it can be observed that the behavior of Zircaloy-2 samples can be drastically different than the two other alloys studied. Indeed, because of the inner liner pumping effect [31, 32], the lower cooling rate modified drastically the hydrogen distribution in the Zircaloy-2 specimens. For Type B treatment (cooling rate around 60 °C/h), the hydrogen distribution remains nearly the same as in the initial, as-irradiated state, whereas for Type C treatments (cooling rate around 6°C/h for Type C TS) more than 85% of the hydrogen is located in the liner or at the liner-Zircaloy-2 interface. These results at 400 °C are fully consistent with those reported in [19] and [33].

Consequently, the difference between Type C and B treatment effects on Zircaloy-2 LK3 cladding is mainly a cooling rate effect on hydride distribution rather than a constant or decreasing pressure effect on hydride reorientation. Recrystallized Zircaloy-2 has also been observed in [1] to be significantly more prone to hydride reorientation than CWSR Zircaloy-4 and Zirlo™. Similar trends were observed in the unirradiated state: Bai et al. [7] reported a much lower HRO critical stress on unirradiated recrystallized Zircaloy-4 than on unirradiated CWSR Zircaloy-4. Consequently, the difference between CWSR Zircaloy-4 and Zirlo™ on one side and recrystallized Zircaloy-2 on the other side may be attributed to the difference in the metallurgical state rather than to a chemical composition effect. Contrary to the grains of recrystallized cladding, the grains of CWSR cladding are elongated in the axial-circumferential direction. In such materials, circumferentially oriented grain boundaries are consequently more numerous than radially oriented grain boundaries. Because part of the hydride precipitation takes place at the grain boundaries [31], the higher HRO critical stress of CWSR materials (with similar crystallographic texture) is likely to be due to a grain shape effect.

Table 4: Oxide fracture and preferential hydride precipitation correlation to creep strain after Type B and C treatments on Zircaloy-4 and Zirlo™ specimens

Material	Treatment temperature and effective stress	Treatment	Creep strain [%]	Outer oxide fracture frequency	Metal fracture	Preferential hydride precipitation at crack tips
Zry-4	400 °C, 120 MPa	B	0.04	a few cracks	no	no
Zirlo™	400 °C, 120 MPa	B	0.03	a few cracks	no	no
Zry-4	350 °C, 111 MPa	C TS	0.03	a few cracks	no	no
Zirlo™	350 °C, 111 MPa	C TS	0.04	a few cracks	no	no
Zry-4	400 °C, 120 MPa	C TS	0.17	every ≈ 180 µm	no	yes, mainly at outer side crack tips
Zirlo™	400 °C, 120 MPa	C TS	0.19	every ≈ 100 µm	one inner side crack (< 10 µm)	yes, mainly at inner side crack tips

5 Conclusions

A distinct effect of irradiation on the critical stress for hydride reorientation, during cooling from the hold temperature under constant pressure, is not readily observable. If an irradiation effect exists, then it is within the precision of the measurements (±10 MPa) for CWSR Zirlo™ and within the effect of the difference in the hydrogen content (±15 MPa) for CWSR Zircaloy-4.

The HRO critical stress, defined as the stress at which hydride reorientation is first observed, is slightly higher for irradiated CWSR Zircaloy-4 than for irradiated CWSR Zirlo™.

Hydride reorientation causes a ductile-to-brittle transition in tensile ring testing at room temperature. In the case of Zirlo™, the ductile-to-brittle transition for the irradiated material occurs at a lower stress range than for the unirradiated material, unlike for Zircaloy-4 where no such effect was apparent.

The extent of hydride reorientation decreases when the stress (internal pressure) is allowed to decrease proportionally with temperature during cooling, even under conditions that involve long durations at the hold temperature and low cooling rate. Decreasing stress scenario is a better simulation of actual field conditions. When hydride re-precipitation first occurs, the effective stress in the cladding specimen is lower than the effective stress obtained in corresponding laboratory experiments performed at constant load (i.e., by maintaining a constant internal pressure when using internal pressurization). Because the temperature at which hydride re-precipitation first occurs is the same, whether the experiment is conducted at constant or decreasing stress, a lower stress state in the specimen therefore decreases the potential for radial hydride precipitation.

Creep strain may lead to cracking of the oxide layer, which can cause preferential hydride precipitation and reorientation in the vicinity of the oxide cracks.

Author contributions

Q. Auzoux : Conceptualization; Investigation; Writing - original draft; Writing - review & editing.

P. Bouffioux : Conceptualization; Investigation; Writing - original draft.

A. Machiels : Conceptualization; Writing - review & editing.

S. Yagnik : Funding acquisition; Project administration; Writing - review & editing

B. Bourdiliau : Investigation;

C. Mallet : Investigation;

N. Mozzani : Formal analysis; Writing - original draft

K. Colas : Writing - original draft, Writing - review & editing

Acknowledgements

This work was carried out under the auspices of the EPRI-led NFIR program. Additional cost-sharing and financial support by CEA, EDF, and EPRI are thankfully acknowledged. The authors wish to sincerely acknowledge the valuable experimental support from D. Leclaire, J. Ilien, S. Allègre, J-F. Lecot, X. Averty, J-C. Droudun, M. Sonnaert, M. Azera, C. Duguay, L. Pasquier, Y. Sibille, C. Dumas, V. Pivetaud, P. Bottin, M. Gennisson, C. Rabourg, L. Gosmain, O. Rabouille, D. Cury, P. Gavoille, and L. Rancoeur. In addition, thanks are also due for many insightful technical discussions with N. Ramasubramanian, R. Adamson, K. Sakamoto, C. Sainte-Catherine, C. Cappelaere, D. Gilbon, and P. Bossis. Authors also appreciate programmatic guidance of the NFIR program under the chairmanship of N. Waeckel and the permission given by the members to publish the results.

References

1. Auzoux, Q., Bouffioux P. , Machiels A., Yagnik S., Bourdiliau B., Mallet C., Mozzani N., Colas K., Hydride reorientation and its impact on room temperature mechanical properties of high burn-up irradiated and unirradiated recrystallized Zircaloy-2. Journal of Nuclear Materials, 2017. 494: p. 114-126.
2. Kearns, J.J., Terminal solubility and partitioning of hydrogen in the alpha phase of zirconium, Zircaloy-2 and Zircaloy-4. Journal of Nuclear Materials, 1967. 22: p. 292-303.
3. Ells, C.E., Hydride precipitates in zirconium alloys (A review). Journal of Nuclear Materials, 1968. 28(2): p. 129-151.
4. Louthan, M.R. and R.P. Marshall, Control of Hydride Orientation in Zircaloy. Journal of Nuclear Materials, 1963. 9(2): p. 170-184.
5. Marshall, R.P. and Louthan Jr., M.R., Tensile properties of Zircaloy with Oriented Hydrides. Trans. Am. Soc. Met., 1963. 56: p. 693-700.
6. Kearns, J.J. and Woods, C.R., Effect of texture, grain size, and cold work on the precipitation of oriented hydrides in Zircaloy tubing and plate. Journal of Nuclear Materials, 1966. 20: p. 241-261.
7. Bai, J., Ji, N., Gilbon, D., Prioul, C. and François, D., Hydride Embrittlement in Zircaloy-4 Plate: Part II. Interaction between the Tensile Stress and the Hydride Morphology. Metallurgical and Materials Transactions A, 1994. 25A: p. 1199-1208
8. Yagnik, S.K., Kuo, R-C, Rashid, Y.R., Machiels, A.J. and Yang R.L., Effect of hydrides on the mechanical properties of Zircaloy-4. in International Meeting on LWR Fuel Performance. 2004. Orlando, Florida, paper 1089.
9. Hong, S.I. and Lee, K.W., Stress-Induced Reorientation of Hydrides and Mechanical Properties of Zircaloy-4 Cladding Tubes. Journal of Nuclear Materials, 2005. 340: p. 203-208.
10. Chu, H.C., Wu, S.K. and Kuo, R.C., Hydride Reorientation in Zircaloy-4 Cladding. Journal of Nuclear Materials, 2008. 373: p. 319-327
11. Singh, R.N., Lala Mikin, R., Dey, G.K., Sah, D.N., Batra, I.S. and Ståhle, P. Influence of temperature on threshold stress for reorientation of hydrides and residual stress variation across thickness of Zr–2.5Nb alloy pressure tube. Journal of Nuclear Materials 2006. 359: p. 208–219
12. Min, S-J., Won, J-J. and Kim, K-T., Terminal cool-down temperature-dependent hydride reorientations in Zr–Nb Alloy claddings under dry storage conditions. Journal of Nuclear Materials 2014, 448: p. 172–183
13. Kim, J-S., Kim, Y-J., Kook, D-H. and Kim, Y-S., A study on hydride reorientation of Zircaloy-4 cladding tube under stress. Journal of Nuclear Materials 2015. 456: p. 246–252
14. Cha, H-J., Won, J-J., Jang, K-N., An, J-H. and Kim, K-T., Tensile hoop stress-, hydrogen content- and cooling rate-dependent hydride reorientation behaviors of Zr alloy cladding tubes. Journal of Nuclear Materials 2015. 464: p. 53–60
15. Lee, J.M., Kim, H-A., Kook, D-H. and Kim, Y.-S., A study on the effects of hydrogen content and peak cladding temperature on threshold stress for hydride reorientation in Zircaloy-4 cladding. Journal of Nuclear Materials, 2018. 509: p. 285-294.
16. Einziger, R.E., Brown, C.L., Hornseth, G.P. and Interrante, C.G., Data Needs for Storage and Transportation of High-Burnup Fuel. Radwaste Solutions, 2005. March-April: p. 44-57.

17. Daum, R.S., Majumdar, S., Liu, Y. and Billone, M.C., Mechanical Testing of High-Burnup Zircaloy-4 Fuel Cladding under Conditions Relevant to Drying Operations and Dry-Cask Storage. in Water Reactor Fuel Performance Meeting. 2005. Kyoto, Japan, paper 1051
18. Daum, R.S., Majumdar, S., Liu, Y. and Billone, M.C., Radial-hydride Embrittlement of High-burnup Zircaloy-4 Fuel Cladding. Journal of Nuclear Science and Technology, 2006. 43(9): p. 1054-1067.
19. Aomi, M., Baba, T., Miyashita, T., Kamimura, K., Yasuda, T., Shinohara Y. and Takeda, T., Evaluation of hydride reorientation behavior and mechanical properties for high-burnup fuel-cladding tubes in interim dry storage. Journal of ASTM International, 2008. 5(9): p. 651-673.
20. Valance, S., Bertsch, J. and Alam, A.M., Statistical Analysis of reorientation properties in irradiated Zircaloy-2, J. ASTM Int., 2011, 8 (1): p. 523-543.
21. Valance, S. and Bertsch, J., Hydrides reorientation investigation of high burn-up PWR fuel cladding, Journal of Nuclear Materials, 2015, 464: p. 371-381.
22. Billone, M.C., Burtseva, T.A. and Einziger, R.E., Ductile-to-brittle transition temperature for high-burnup cladding alloys exposed to simulated drying-storage conditions. Journal of Nuclear Materials, 2013, 433: p. 431-448.
23. Method of analyzing an image of hydrides in a metal alloy, in particular in a nuclear fuel cladding alloy, European Patent EP 2 232 438 B1.
24. Kammenzind, B.F., Franklin, D.G., Peters, H.R. and Duffin, W.J., Hydrogen Pickup and Redistribution in Alpha-Annealed Zr-4. in Zirconium in the Nuclear Industry: 11th International Symposium. 1996. ASTM.
25. Daum, R.S., Majumdar, S., Bates, D. W., Motta, A. T., Koss, D. A. and Billone, M. C., On the embrittlement of Zircaloy-4 under RIA-relevant conditions. in Zirconium in the Nuclear Industry: 13th International Symposium. 2002. ASTM.
26. Puls, M.P., in: The Effect of Hydrogen and Hydrides on the Integrity of Zirconium Alloy Components, Engineering Materials, Springer-Verlag, London, 2012.
27. Colas, K., Motta, A., Daymond, M. R. and Almer, J., Mechanisms of Hydride Reorientation in Zircaloy-4 Studied in Situ. Zirconium in the Nuclear Industry: 17th International Symposium, 2014, ASTM: p. 1107–1137.
28. Lacroix, E., Simon, P.-C. A., Motta, A.T. and Almer J.D., Zirconium Hydride Precipitation and Dissolution Kinetics in Zirconium Alloys. Zirconium in the Nuclear Industry: 19th International Symposium, 2021. ASTM: p. 67-91.
29. Lacroix, E., Motta, A.T. and Almer, J.D., Experimental determination of zirconium hydride precipitation and dissolution in zirconium alloy. Journal of Nuclear Materials, 2018. 509: p. 162-167.
30. Passelaigue, F., Lacroix, E., Pastore, G. and Motta, A.T., Implementation and Validation of the Hydride Nucleation-Growth-Dissolution (HNGD) model in BISON, Journal of Nuclear Materials, 2021. 544: 152683
31. Une, K., Ishimoto, S., Etoh, Y., Ito, K., Ogata, K., Baba, T., Kamimura, K. and Kobayashi, Y., The terminal solid solubility of hydrogen in irradiated Zircaloy-2 and microscopic modeling of hydride behavior. Journal of Nuclear Materials, 2009. 389: p. 127-136.
32. Une, K. and Ishimoto, S., Terminal Solid Solubility of Hydrogen in unalloyed Zirconium by Differential Scanning Calorimetry. Journal of Nuclear Science and Technology, 2004. 41: p. 249.

33. Sakamoto, K., Matsuoka, H., Takagi, A. and Kashibe, S., Study on Hydride Reorientation in Zry-2 Fuel Cladding during Interim Dry Storage. in International LWR Fuel Performance Meeting. 2007. San Francisco, CA., paper 1016.